Chemistry–A European Journal

Supporting Information

Modulating the Shape of Short Metal-Mediated Heteroleptic Tapes of Porphyrins

Alessio Vidal, Daniel Rossato, Elisabetta Iengo, Gabriele Balducci, and Enzo Alessio*

- Additional information on the intermediates [{*t*,*c*,*c*-$RuCl_2(CO)_2$(dmso-O)}$_2$(3′*cis*DPyMP)] (**4**) and [{*t*,*c*,*c*-$RuCl_2(CO)_2$(dmso-O)}$_2$(4′*cis*DPyMP)] (**5**).

  Scheme S1. Preparation of **4** and **5**.

  Figures S1 – S3. Mono and bidimensional ^{1}H NMR spectra for **4** and **5**.

- Preparation and spectroscopic characterization of tape [{t,c,c-$RuCl_2(CO)_2$}$_4$(4′cisDPyMP)$_2$(4′TPyP)] (**D_4-T_4-D_4**).

  Scheme S2. Preparation of **D_4-T_4-D_4**.

  Figure S4. ^{1}H NMR spectrum ($CDCl_3$) of **D_4-T_4-D_4** with labelling scheme.

- Additional information on tape [{*t*,*c*,*c*-$RuCl_2(CO)_2$}$_4$(3′*cis*DPyMP)$_2$(4′TPyP)] (**D_3-T_4-D_3**).

  Scheme S3. Preparation of **D_3-T_4-D_3**.

  Figures S5 – S10. 2D NMR spectra of tape [{*t*,*c*,*c*-$RuCl_2(CO)_2$}$_4$(3′*cis*DPyMP)$_2$(4′TPyP)] (**D_3-T_4-D_3**).

  Figure S11. Normalized UV-Vis absorption spectrum ($CHCl_3$) of tape [{*t*,*c*,*c*-$RuCl_2(CO)_2$}$_4$(3′*cis*DPyMP)$_2$(4′TPyP)] (**D_3-T_4-D_3**).

- Additional information on tape [{*t*,*c*,*c*-$RuCl_2(CO)_2$}$_4$(4′*cis*DPyMP)$_2$(3′TPyP)] (**D_4-T_3-D_4**) and [{*t*,*c*,*c*-$RuCl_2(CO)_2$}$_4$(Zn·4′*cis*DPyMP)$_2$(Zn·3′TPyP)] (**ZnD_4-ZnT_3-ZnD_4**).

  Scheme S4. Preparation of **D_4-T_3-D_4**.

  Figures S12 – S16. 1D and 2D NMR spectra of tape [{*t*,*c*,*c*-$RuCl_2(CO)_2$}$_4$(4′*cis*DPyMP)$_2$(3′TPyP)] (**D_4-T_3-D_4**).

  Figure S17. Normalized UV-Vis absorption spectrum ($CHCl_3$) of tape [{*t*,*c*,*c*-$RuCl_2(CO)_2$}$_4$(4′*cis*DPyMP)$_2$(3′TPyP)] (**D_4-T_3-D_4**).

  Figure S18. Normalized UV-Vis absorption spectrum ($CHCl_3$) of tape [{*t*,*c*,*c*-$RuCl_2(CO)_2$}$_4$(Zn·4′*cis*DPyMP)$_2$(Zn·3′TPyP)] (**ZnD_4-ZnT_3-ZnD_4**).

- Additional information on tapes [{*t*,*c*,*c*-$RuCl_2(CO)_2$}$_4$(3′*cis*DPyMP)$_2$(3′TPyP)] (**D_3-T_3-D_3**) and [{*t*,*c*,*c*-$RuCl_2(CO)_2$}$_4$(Zn·3′*cis*DPyMP)$_2$(Zn·3′TPyP)] (**ZnD_3-ZnT_3-ZnD_3**).

  Scheme S5. Preparation of **D_3-T_3-D_3**.

  Figures S19 – S21. 2D NMR spectra of tape [{*t*,*c*,*c*-$RuCl_2(CO)_2$}$_4$(3′*cis*DPyMP)$_2$(3′TPyP)] (**D_3-T_3-D_3**).

  Figure S22. CO stretching region in the IR spectrum ($CHCl_3$) of tape [{*t*,*c*,*c*-$RuCl_2(CO)_2$}$_4$(3′*cis*DPyMP)$_2$(3′TPyP)] (**D_3-T_3-D_3**).

  Figure S23. Normalized UV-Vis absorption spectrum ($CHCl_3$) of tape [{*t*,*c*,*c*-$RuCl_2(CO)_2$}$_4$(Zn·3′*cis*DPyMP)$_2$(Zn·3′TPyP)] (**ZnD_3-ZnT_3-ZnD_3**).

Additional comments on the preparation and spectroscopic characterization of the ditopic reactive intermediates [{*t,c,c*-$RuCl_2(CO)_2$(dmso-O)}$_2$(3′*cis*DPyMP)] (4) and [{*t,c,c*-$RuCl_2(CO)_2$(dmso-O)}$_2$(4′*cis*DPyMP)] (5).

The two ditopic reactive intermediates [{*t,c,c*-$RuCl_2(CO)_2$(dmso-O)}$_2$(3′*cis*DPyMP)] (**4**) and [{*t,c,c*-$RuCl_2(CO)_2$(dmso-O)}$_2$(4′*cis*DPyMP)] (**5**) were prepared as summarized in Scheme S1. The isolation of these compounds involves washing the crudes with water to remove the unreacted ruthenium complex and the released DMSO (the products are soluble in all the other solvents tested). As explained for the corresponding phenyl derivatives previously described by us [46], the washing removes also part of the bound dmso-O, thus affording mixtures that – besides **4** or **5** – contain mainly the corresponding aqua species, [{*t,c,c*-$RuCl_2(CO)_2(OH_2)$}$_2$(3′*cis*DPyMP)] (**4H_2O**) and [{*t,c,c*-$RuCl_2(CO)_2(OH_2)$}$_2$(4′*cis*DPyMP)] (**5H_2O**), respectively. The presence of such mixtures is apparent in the ^{1}H NMR spectra in $CDCl_3$. However, when the crude reaction products are dissolved in DMSO-d_6 the coordinated water is replaced by the solvent and the ^{1}H NMR spectrum presents only one main set of resonances for each compound, consistent with 3′- (for **4**) or 4′*cis*DPyP (for **5**) being symmetrically coordinated to two equal Ru(II) complexes (Figures S1 – S3). Since from the point of view of the further reactivity the dmso-O and the aquo species behave equally, and the influence on the M_W and stoichiometric ratio of the reactions is marginal, for the sake of simplicity in the text no distinction between them is made and only the labels **4** and **5** are used.

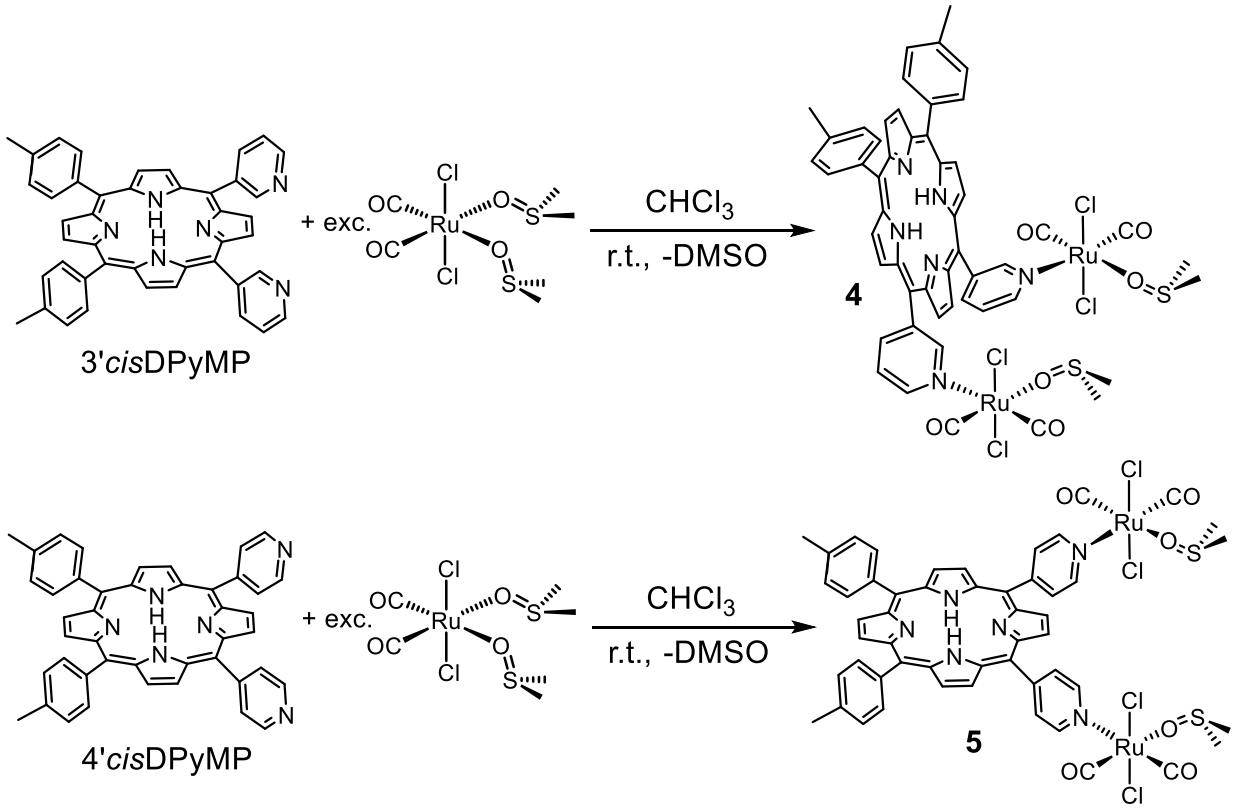

Scheme S1. The preparations of the reactive intermediates [{*t*,*c*,*c*-$RuCl_2(CO)_2$(dmso-O)}$_2$(3′*cis*DPyMP)] (**4**) and [{*t*,*c*,*c*-$RuCl_2(CO)_2$(dmso-O)}$_2$(4′*cis*DPyMP)] (**5**).

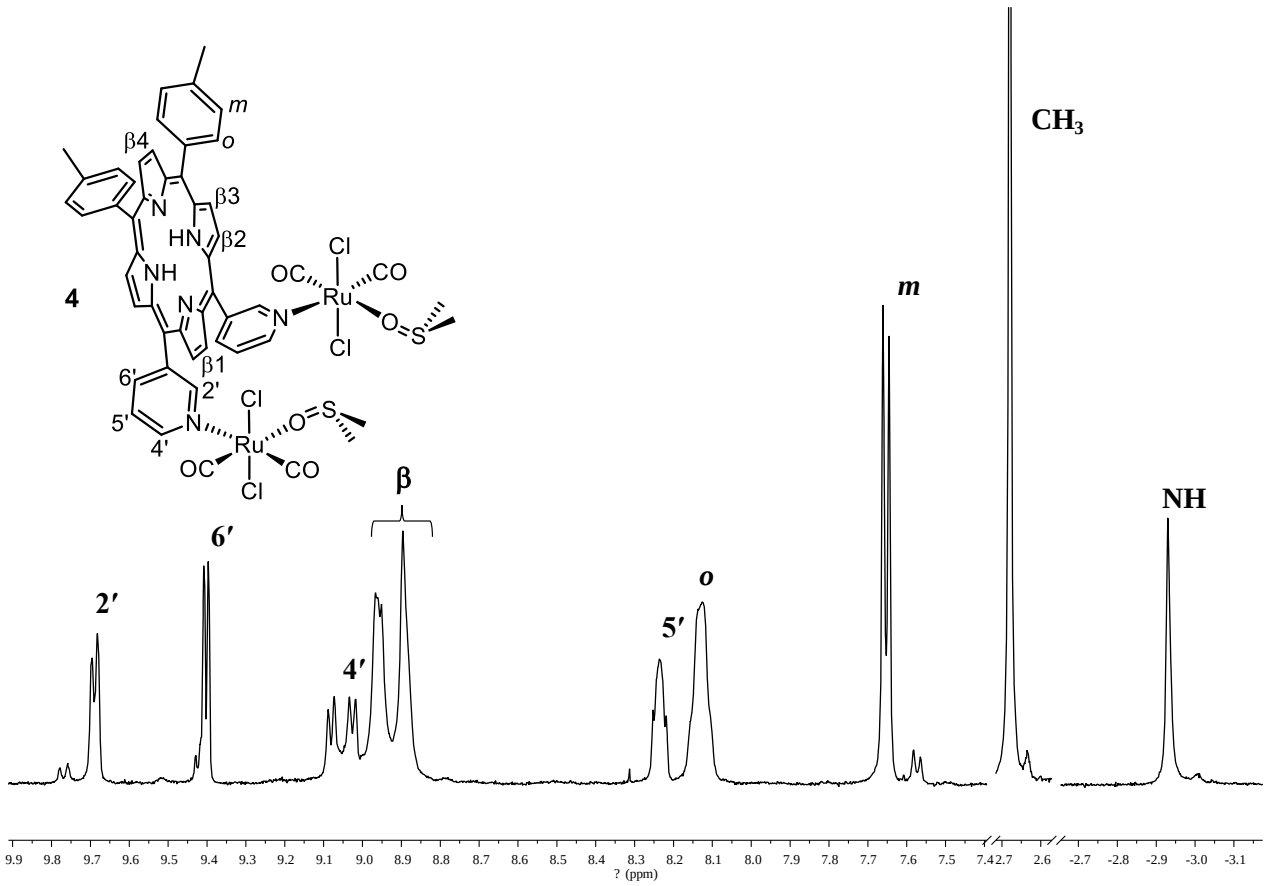

Figure S1. ^{1}H NMR spectrum (DMSO-d_6) of [{*t*,*c*,*c*-$RuCl_2(CO)_2$(dmso-O)}$_2$(3′*cis*DPyMP)] (**4**) with labelling scheme.

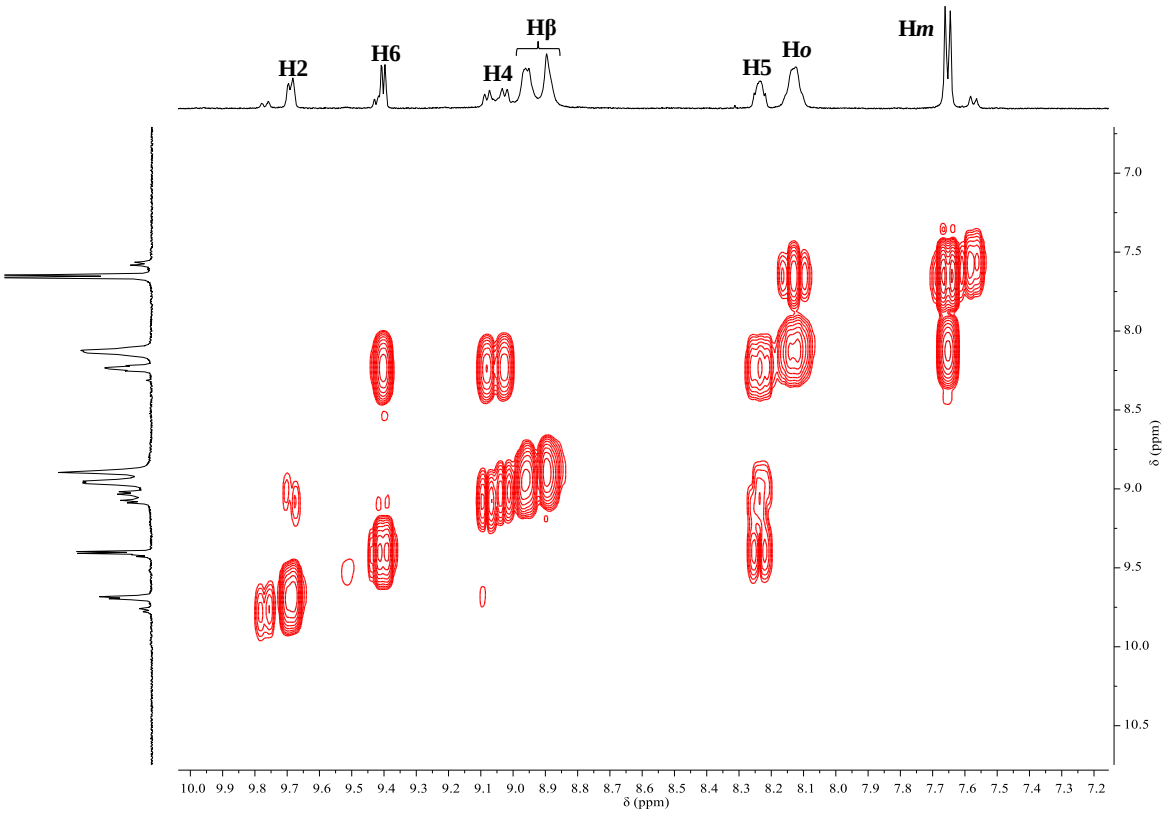

Figure S2. H-H COSY NMR spectrum (aromatic region, DMSO-d_6) of [{*t*,*c*,*c*-$RuCl_2(CO)_2$(dmso-O)}$_2$(3′*cis*DPyMP)] (**4**). See Figure S1 for labelling scheme.

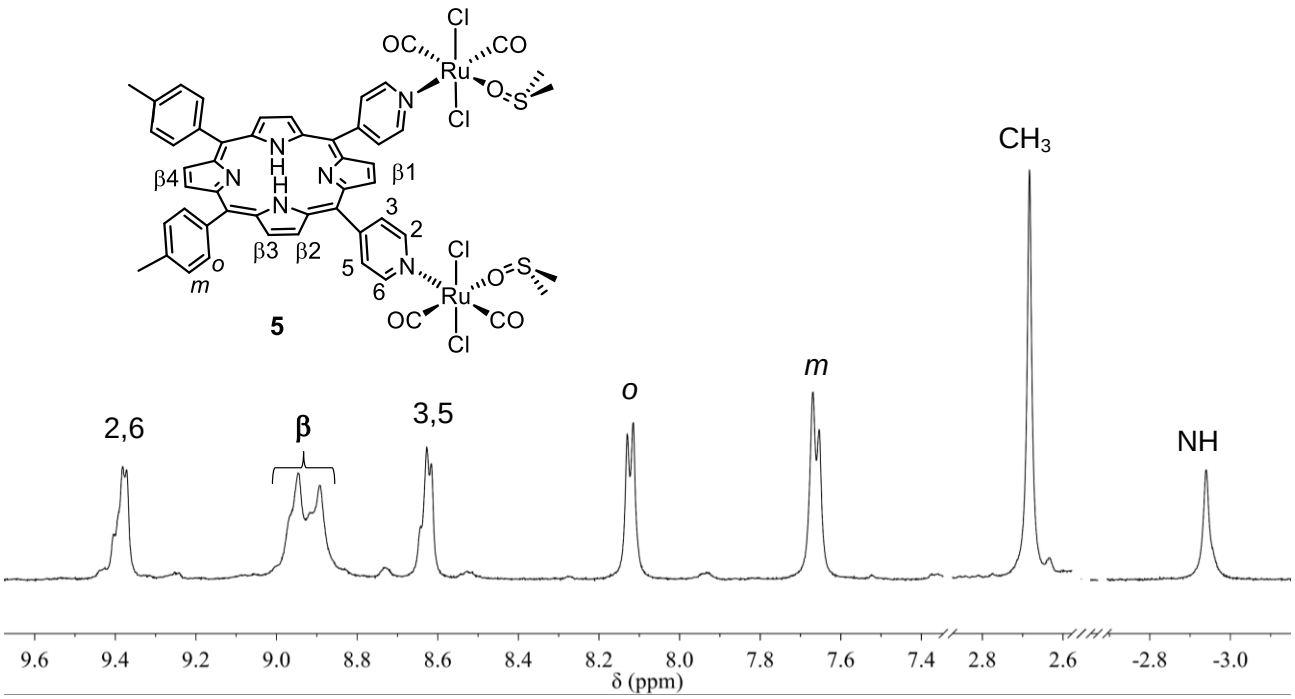

Figure S3. ^{1}H NMR spectrum (DMSO-d_6) of [{*t*,*c*,*c*-$RuCl_2(CO)_2$(dmso-O)}$_2$(4′*cis*DPyMP)] (**5**) with labelling scheme.

Tape [{*t,c,c*-$RuCl_2(CO)_2$}$_4$(4′*cis*DPyMP)$_2$(4′TPyP)] (D_4-T_4-D_4).

Contrary to our expectations, the geometrically simplest tape [{*t,c,c*-$RuCl_2(CO)_2$}$_4$(4′*cis*DPyMP)$_2$(4′TPyP)] (**D_4-T_4-D_4**), for which no stereoisomers are predicted, turned out to be the most difficult to obtain in pure form, due to its low solubility in chlorinated solvents, most likely attributable to its flat geometry leading to strong stacking interactions.

Treatment of **5** with ca. 0.5 equiv. of 4′TPyP (Scheme S2) yielded a purple solid that, after chromatographic purifications, afforded a very small amount of pure compound that was barely sufficient for basic NMR characterization. In fact, even though the fractions eluted from the column were transparent solutions, removal of the solvent afforded purple precipitates that turned out to be only sparingly soluble in $CDCl_3$ or CD_2Cl_2, affording turbid suspensions Furthermore, even when the precipitate was removed by filtration, soon the clear solution became turbid again with formation of a very fine purple precipitate. The straightforward ^{1}H NMR spectrum of the purified product (Figure S4) shows the presence of a single, very symmetrical compound, and is fully consistent with the expected nature of the **D_4-T_4-D_4** tape, with only two types of 4′pyridyl rings, four belonging to the central 4′TPyP and four to the two peripheral 4′*cis*DPyP's. The two pairs of equally intense sharp doublets, pairwise correlated in the COSY spectrum, belong to the H2,6 and H3,5 protons (as anticipated, the flat geometry of this tape makes its two sides undistinguishable). We were unable to distinguish which signals belong to 4′TPyP protons and which to the two equivalent 4′*cis*DPyP's. The singlets of the inner NH protons partially overlap at ca. –2.70 ppm, i.e. a chemical shift very similar to that found in the 2+2 homoleptic metallacyle [{*t,c,c*-$RuCl_2(CO)_2$}$_2$(4′*cis*DPyP)$_2$] (**2**), in agreement with a flat geometry and no significant mutual shielding of the three porphyrins.

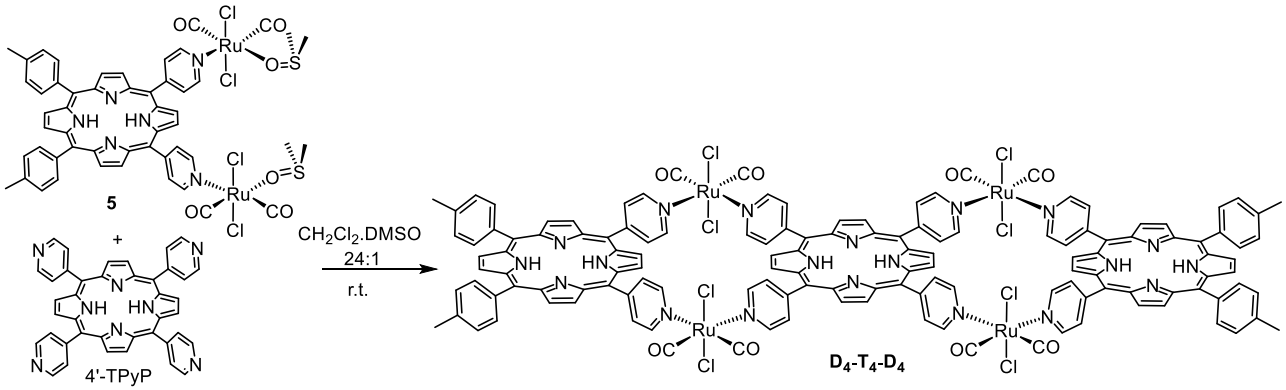

Scheme S2. The preparation of tape **D_4-T_4-D_4**.

Preparation of [{*t,c,c*-$RuCl_2(CO)_2$}$_4$(4′*cis*DPyP)$_2$(4′TPyP)] (D_4-T_4-D_4). A 11.1 mg amount of 4′TPyP (0.018 mmol) was partially dissolved in 20 mL of CH_2Cl_2. Prior to the addition of a 56 mg amount of **5** (0.045 mmol, 2.5 equiv.), the purple suspension was heated to reflux for 15 min to

promote the solubilization of the 4′TPyP and then rapidly cooled to room temperature. The mixture was stirred at room temperature, monitored by silica gel TLC ($CHCl_3$:EtOH 97.5:2.5), and stopped after 48 h. The solvent was then removed under reduced pressure and the solid was suspended in acetone and centrifuged (5 min, 5500 rpm × 5) and the supernatant was removed. The solid was purified by column chromatography (silica gel, $CHCl_3$). The first purple band eluted from the column was found to contain the desired product. Removal of the solvent under reduced pressure afforded a purple precipitate (yield 4.5 mg, 9%), that however was only sparingly soluble in $CDCl_3$ and the suspension was filtered prior to NMR analysis. ^{1}H NMR ($CDCl_3$), primed labels indicate protons of the same set of undistinguishable pyridyl rings, either belonging to 4′TPyP or to 4′*cis*DPyP's (see also Figure S4 for the numbering scheme), δ (ppm): 9.93 and 9.85 (2d, 8+8H, 2,6+2′,6′), 9.30–8.86 (singlets and dublets, 24H, β+β′), 8.63 and 8.59 (2d, 8+8H, 3,5+3′,5′), 8.27 (d, 8H, *o*), 7.86 (m, 8H, *m*), 2.77 (s, 12H, CH_3), –2.70 (2s, 6H, NH). UV–vis [$CHCl_3$; λ_{max} (nm), relative intensity (%)]: 426 (100, Soret band), 517 (7.7), 553 (4.23), 590 (3.01), 645 (1.92). IR (selected bands in $CHCl_3$, cm^{-1}): 2075 (ν_{CO}), 2016 (ν_{CO}). TLC R_f ($CHCl_3$) = 0.24.

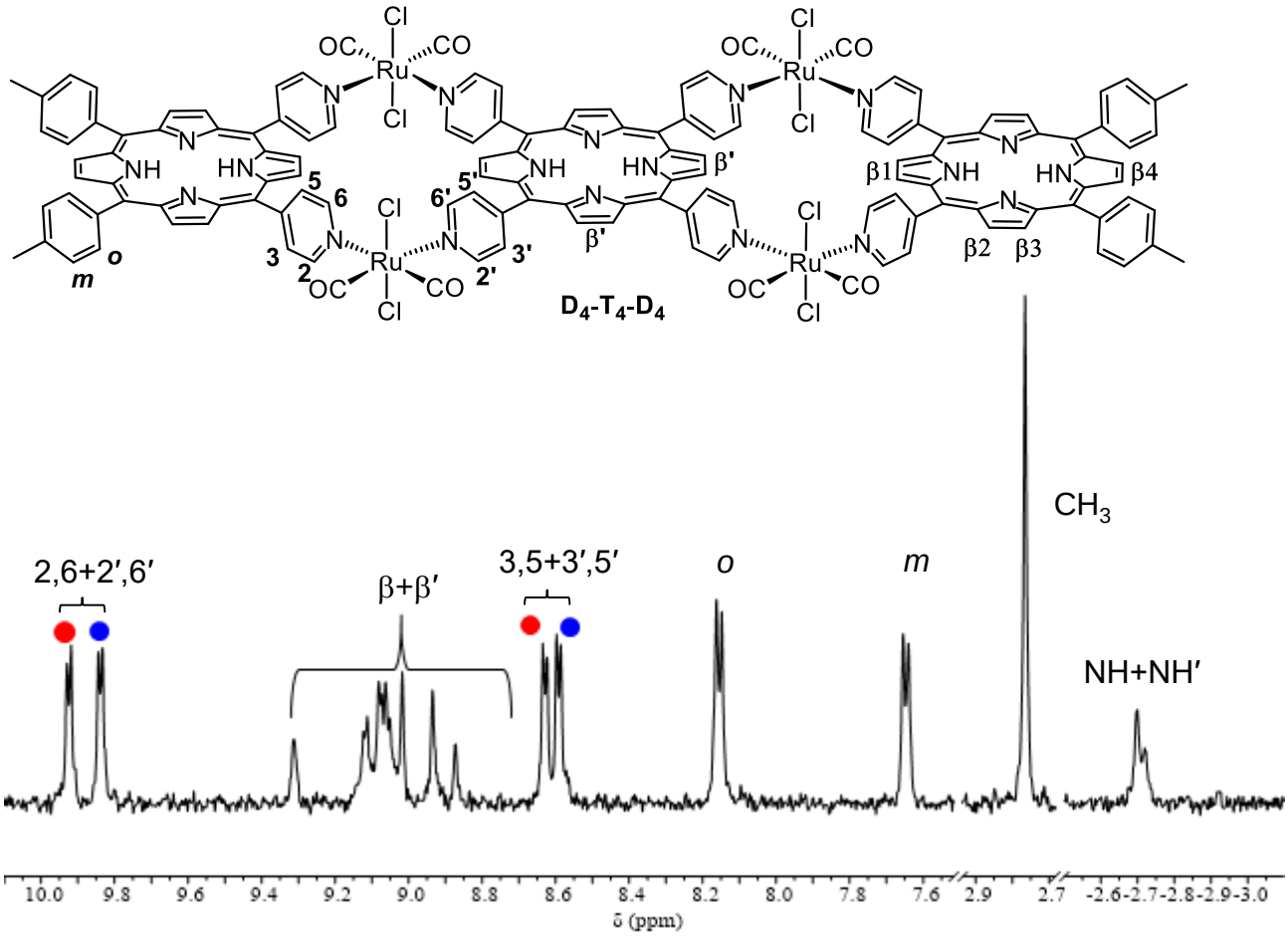

Figure S4. ^{1}H NMR spectrum ($CDCl_3$) of tape [{*t*,*c*,*c*-$RuCl_2(CO)_2$}$_4$(4′*cis*DPyMP)$_2$(4′TPyP)] (**D_4-T_4-D_4**) with labelling scheme. Primed labels formally belong to protons of the central 4′TPyP. Colored dots indicate resonances of protons belonging to the same type of porphyrin, either 4′*cis*DPyMP or 4′TPyP.

Tape [{*t,c,c*-$RuCl_2(CO)_2$}$_4$(3′*cis*DPyMP)$_2$(4′TPyP)] (D_3-T_4-D_3).

Treatment of **4** with ca. 0.5 equiv. of 4′TPyP (Scheme S3) yielded a purple solid that, after chromatographic purification, afforded a very small amount of pure compound.

Details of NMR characterization (Scheme S3 for the labeling scheme): The highest frequency resonances in the ^{1}H NMR spectrum of [{*t,c,c*-$RuCl_2(CO)_2$}$_4$(3′*cis*DPyMP)$_2$(4′TPyP)] (**D_3-T_4-D_3**) are those of the protons H2′ and H6′ of the two equivalent 3′*cis*DPyMP's (a broad singlet and a doublet, respectively). In the H-H COSY spectrum (Figure S5) the long-range cross peak between H2′ and H6′ is in a light-purple frame. As said in the text, in both stereoisomers the 4′-pyridyl protons on the same side of the adjacent orthogonal 3′*cis*DPyMP (H6 and H5 in the convention adopted by us) are more shielded and thus resonate at lower frequencies than the corresponding protons on the other side of the ring (H2 and H3). Their resonances are pairwise connected in the COSY spectrum (Figure S5, H2/H3 blue frame, H5/H6 green frame). Finally, the correlation cross peak between the resonances of the *ortho* and *meta* tolyl protons has an orange frame. The enlargement of the COSY spectrum of Figure S6 shows the cross peaks between the resonances of the pyrrole protons βH and the NH singlets mentioned in the text. The assignments of the resonances of the pyridyl and tolyl protons are confirmed in the HSQC spectrum in Figure S7 as well as by the NOE cross peaks (in red) between the resonances of the pyrrole protons and those of the adjacent pyridyl and/or tolyl protons in the ROESY spectrum (Figure S8). In detail, for the βH signals of 3′*cis*DPyMP's (cross peaks in green frames in the ROESY spectrum): 1) the multiplet at 9.07 ppm was assigned to pyrrole protons Hβ2 and Hβ3 as it correlates with the resonances of H*o* and H2′ (both isomers); 2) the singlet at 8.98 ppm was assigned to Hβ1 as it correlates with the resonances of protons H2′ and H4′. In addition, it has a cross peak with the singlet of Hβ1′ of 4′TPyP at 7.30 ppm; 3) the singlet at 8.68 ppm, that has cross peaks with the resonances of tolyl H*o* and H*m*, was assigned to Hβ4.

In the same ROESY spectrum (Figure S8), the Hβ′ singlets of 4′TPyP (two for each stereoisomer) have cross peaks with the H3 and H5 resonances (light-blue frames); however, the singlet of the major isomer at 7.26 ppm was unambiguously assigned to Hβ1′ because: 1) this proton is more shielded by the adjacent 3′*cis*DPyMP, and 2) it has an NOE cross peak with the resonance of Hβ1 and H2′. As a consequence, the two singlets at 8.83 and 8.73 ppm were assigned to Hβ2′ (both isomers). An enlargement of the ROESY spectrum showing the NOE cross peaks of Hβ1′ of the major isomer is shown in Figure S9. The inset of Figure S8 shows the intramolecular exchange cross peaks (blue) between the doublets of H2 and H6 for both stereoisomers. The other potential exchange cross peaks (e.g. those concerning the resonances of H3 and H5) fall too close to the diagonal for being distinguishable. An intermolecular exchange cross peak between the H6 doublets

of the two stereoisomers was observed (even though very close to the diagonal due to the small chemical shift difference) in the ROESY spectrum recorded at 50°C (and with a mixing time increased to 200 ms) (Figure S10).

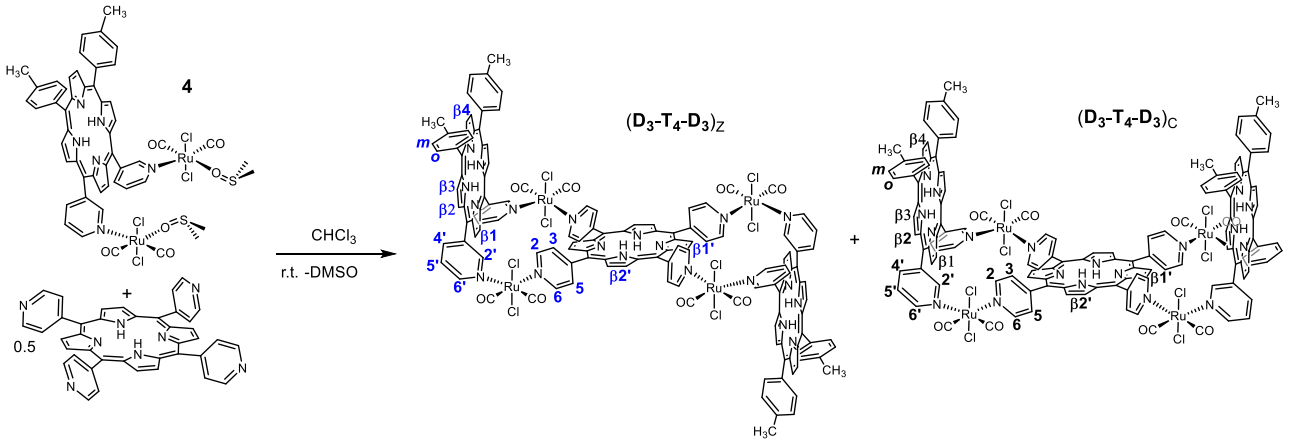

Scheme S3. The preparation of the two stereoisomers of tape [{*t*,*c*,*c*-$RuCl_2(CO)_2$}$_4$(3′*cis*DPyMP)$_2$(4′TPyP)] (**D$_3$-T$_4$-D$_3$**): Z-shaped, (**D$_3$-T$_4$-D$_3$**)$_Z$, and C-shaped, (**D$_3$-T$_4$-D$_3$**)$_C$ with labelling scheme.

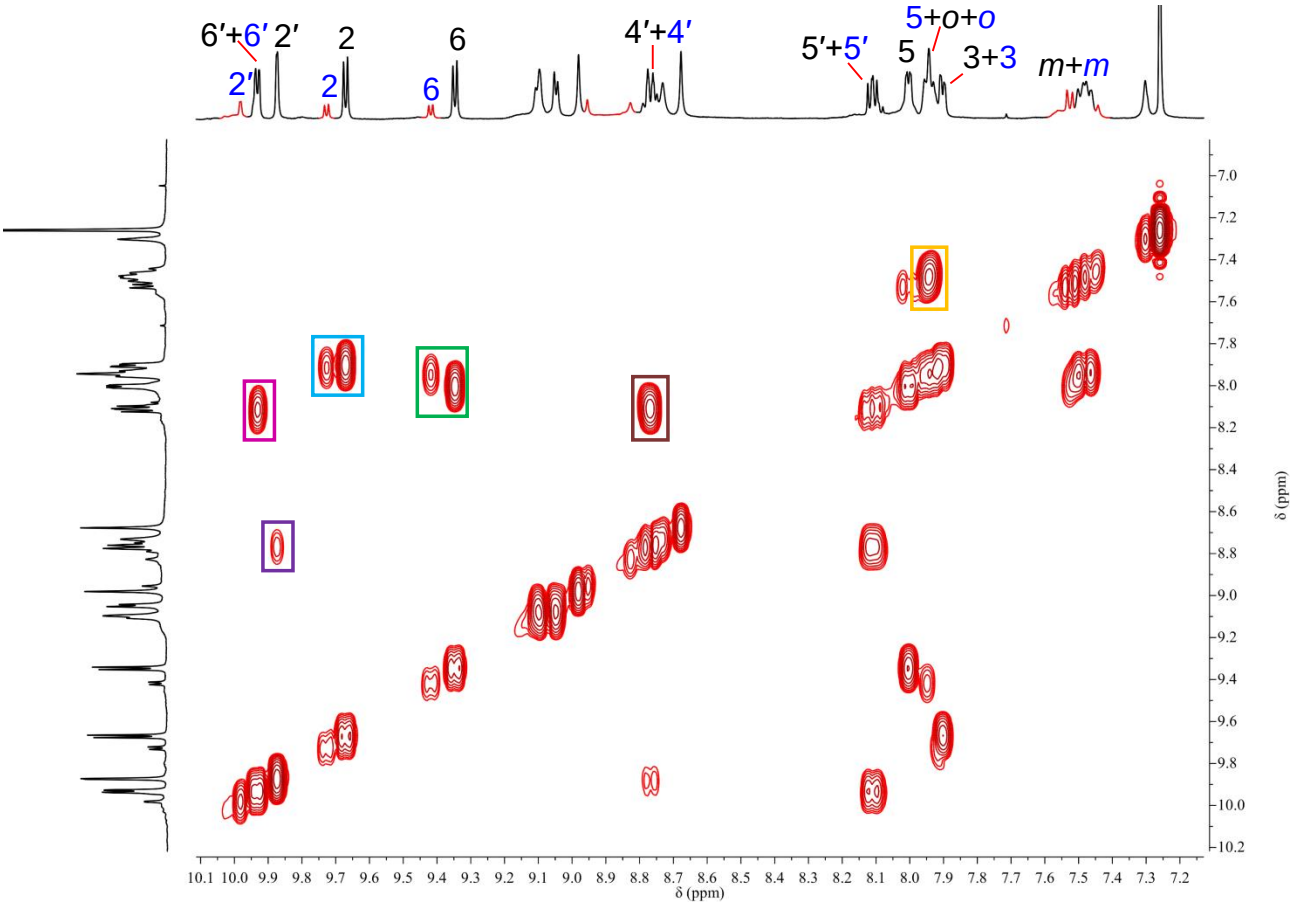

Figure S5. H-H COSY NMR spectrum (aromatic region, $CDCl_3$) of the two stereoisomers of tape [{*t*,*c*,*c*-$RuCl_2(CO)_2$}$_4$(3′*cis*DPyMP)$_2$(4′TPyP)] (**D$_3$-T$_4$-D$_3$**). See Scheme S3 for the labeling scheme. The resonances of the minor isomer, presumably belonging to (**D$_3$-T$_4$-D$_3$**)$_Z$, are in red. The resonances of the minor isomer (in red), attributed to (**D$_3$-T$_4$-D$_3$**)$_Z$, are labeled in blue. In both sets, primed βH and NH labels belong to the central 4′TPyP.

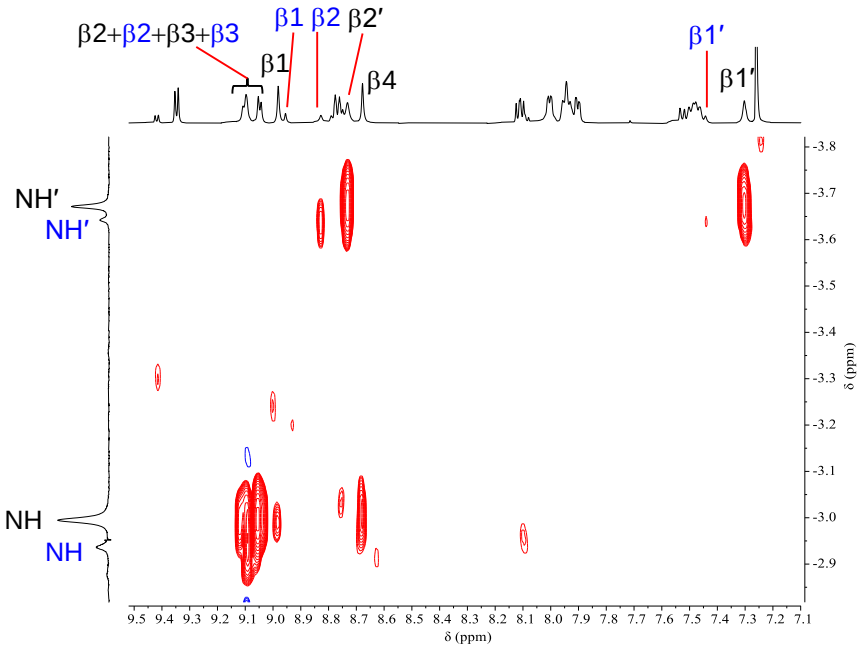

Figure S6. Enlargement of the H-H COSY NMR spectrum ($CDCl_3$) of the two stereoisomers of tape [{*t*,*c*,*c*-$RuCl_2(CO)_2$}$_4$(3′*cis*DPyMP)$_2$(4′TPyP)] (**D_3-T_4-D_3**) showing the couplings between NH singlets and βH resonances. See Scheme S3 for the labeling scheme. In both sets, primed βH and NH labels belong to the central 4′TPyP.

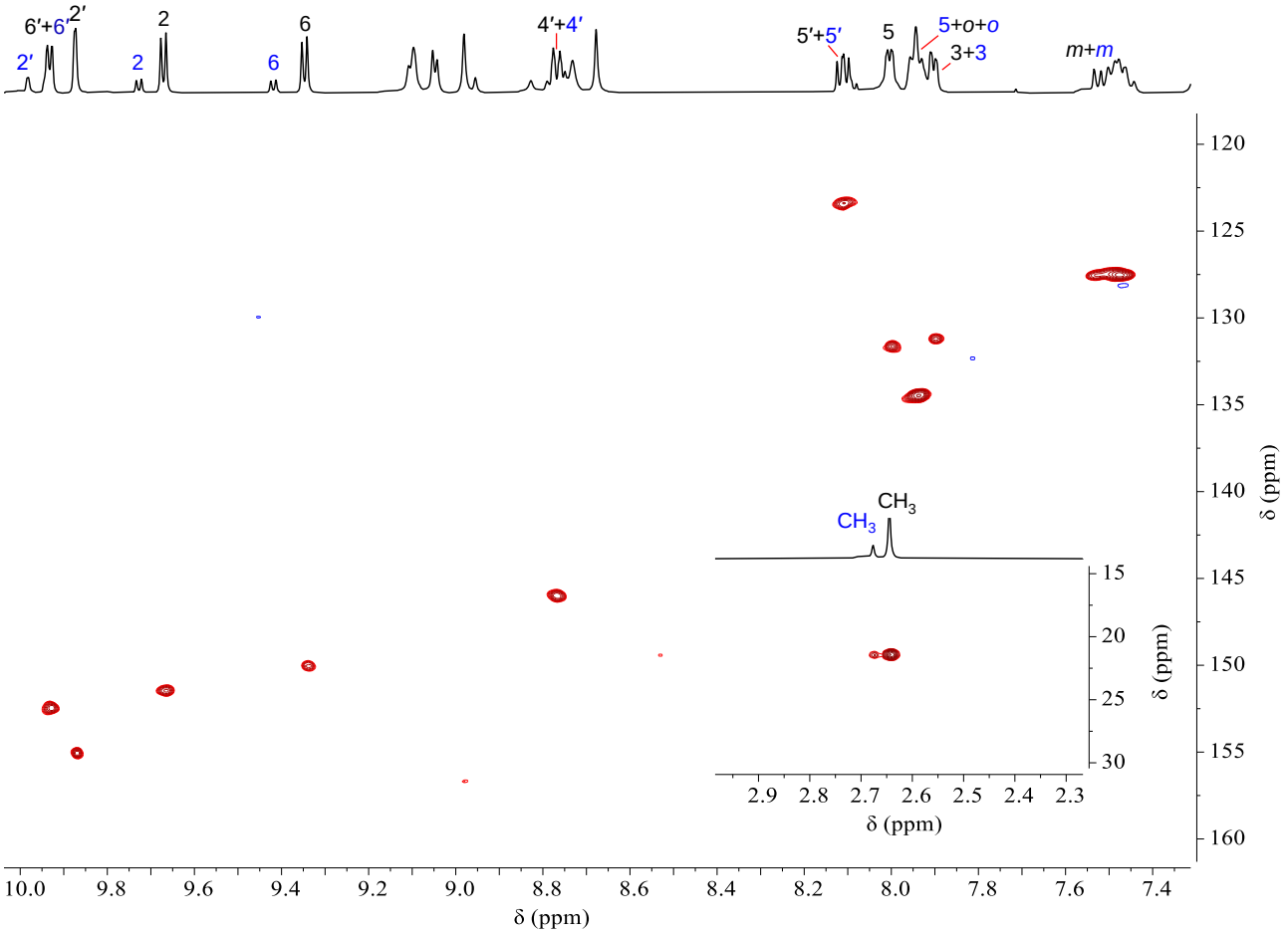

Figure S7. HSQC NMR spectrum ($CDCl_3$) of the two stereoisomers of tape [{*t*,*c*,*c*-$RuCl_2(CO)_2$}$_4$(3′*cis*DPyMP)$_2$(4′TPyP)] (**D_3-T_4-D_3**). For labeling scheme see Scheme S3. In both sets, primed βH and NH labels belong to the central 4′TPyP. The resonances of the minor isomer, presumably belonging to (**D_3-T_4-D_3**)$_Z$, are in blue.

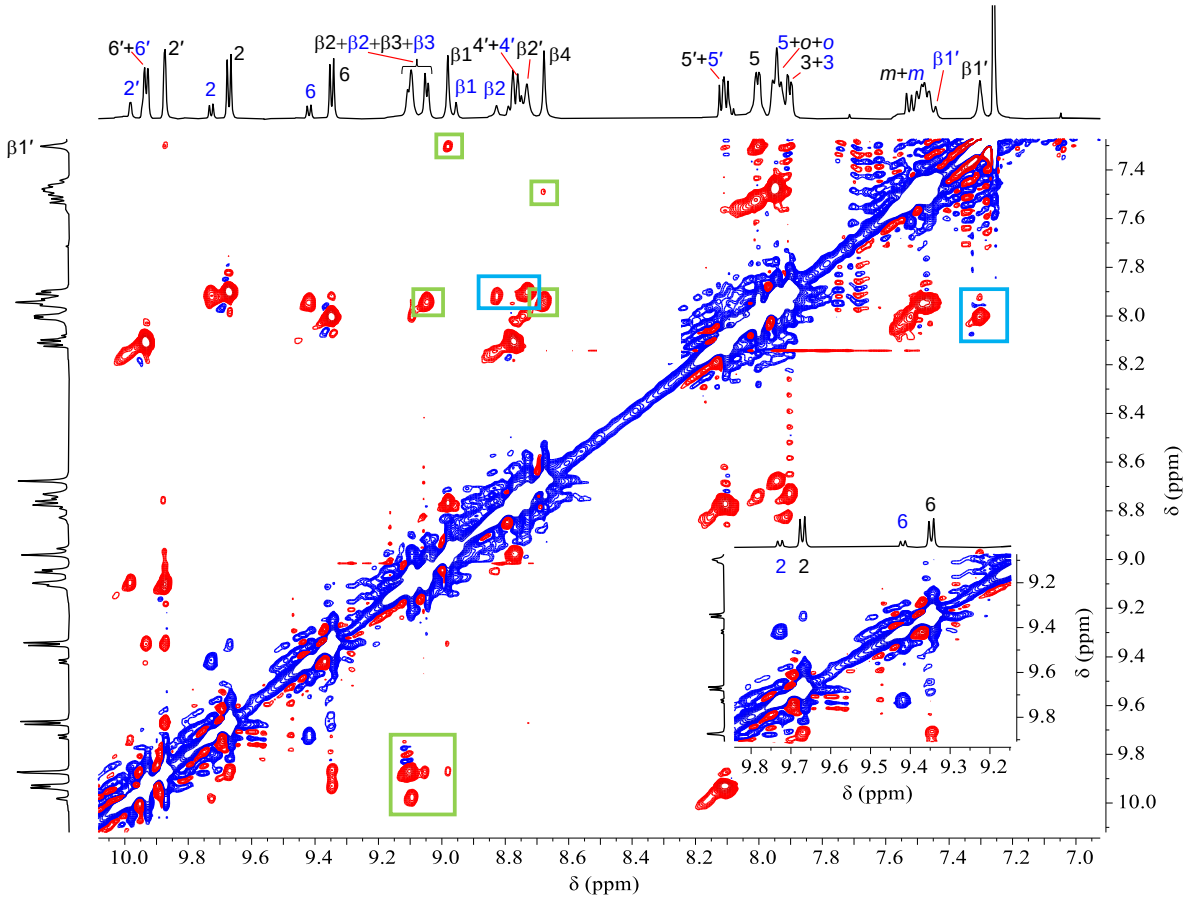

Figure S8. ROESY NMR spectrum ($CDCl_3$) of the two stereoisomers of tape [{*t*,*c*,*c*-$RuCl_2(CO)_2$}$_4$(3′*cis*DPyMP)$_2$(4′TPyP)] (**D_3-T_4-D_3**). See Scheme S3 for the labeling scheme. In both sets, primed βH labels belong to the central 4′TPyP. The resonances of the minor isomer, presumably belonging to (**D_3-T_4-D_3**)$_Z$, are labeled in blue. The NOE cross peaks are red. Green frames for protons of 3′*cis*DPyMP's, blue frame for protons of 4′TPyP. The inset shows intramolecular exchange cross peaks (blue) due to slow rotation of the 4′-pyridyl rings about the about the C_{meso}–C_{ring} bond.

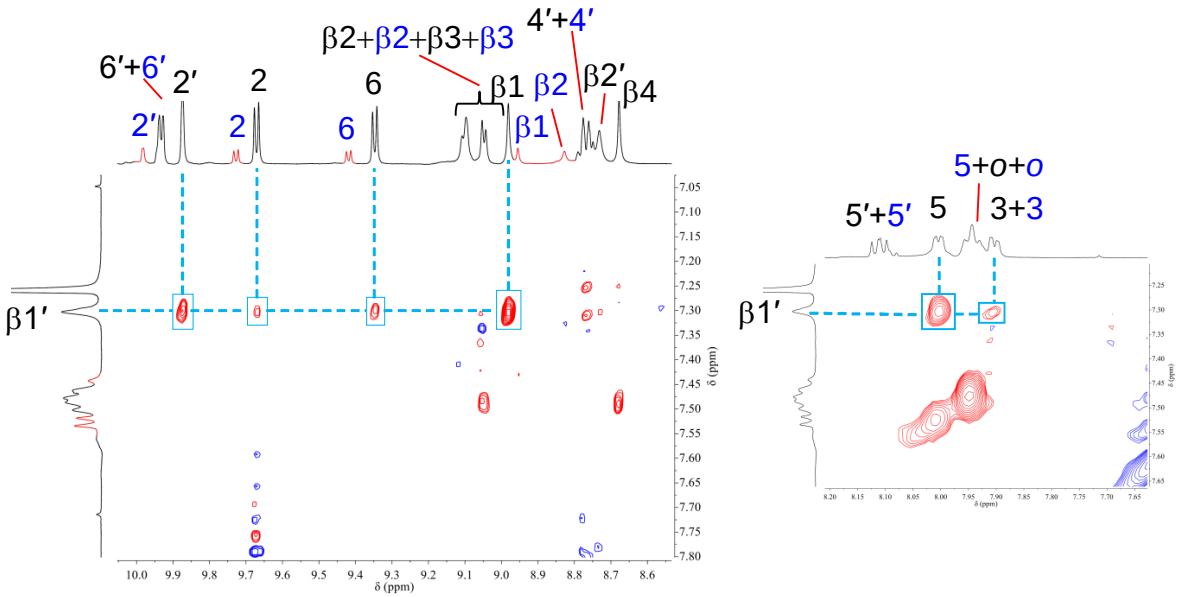

Figure S9. Enlargement of the ROESY NMR spectrum ($CDCl_3$) of the two stereoisomers of tape [{*t*,*c*,*c*-$RuCl_2(CO)_2$}$_4$(3′*cis*DPyMP)$_2$(4′TPyP)] (**D_3-T_4-D_3**) focused on the NOE cross peaks of Hβ1′ of the major isomer. See Scheme S3 for the labeling scheme. In both sets, primed βH labels belong to the central 4′TPyP.

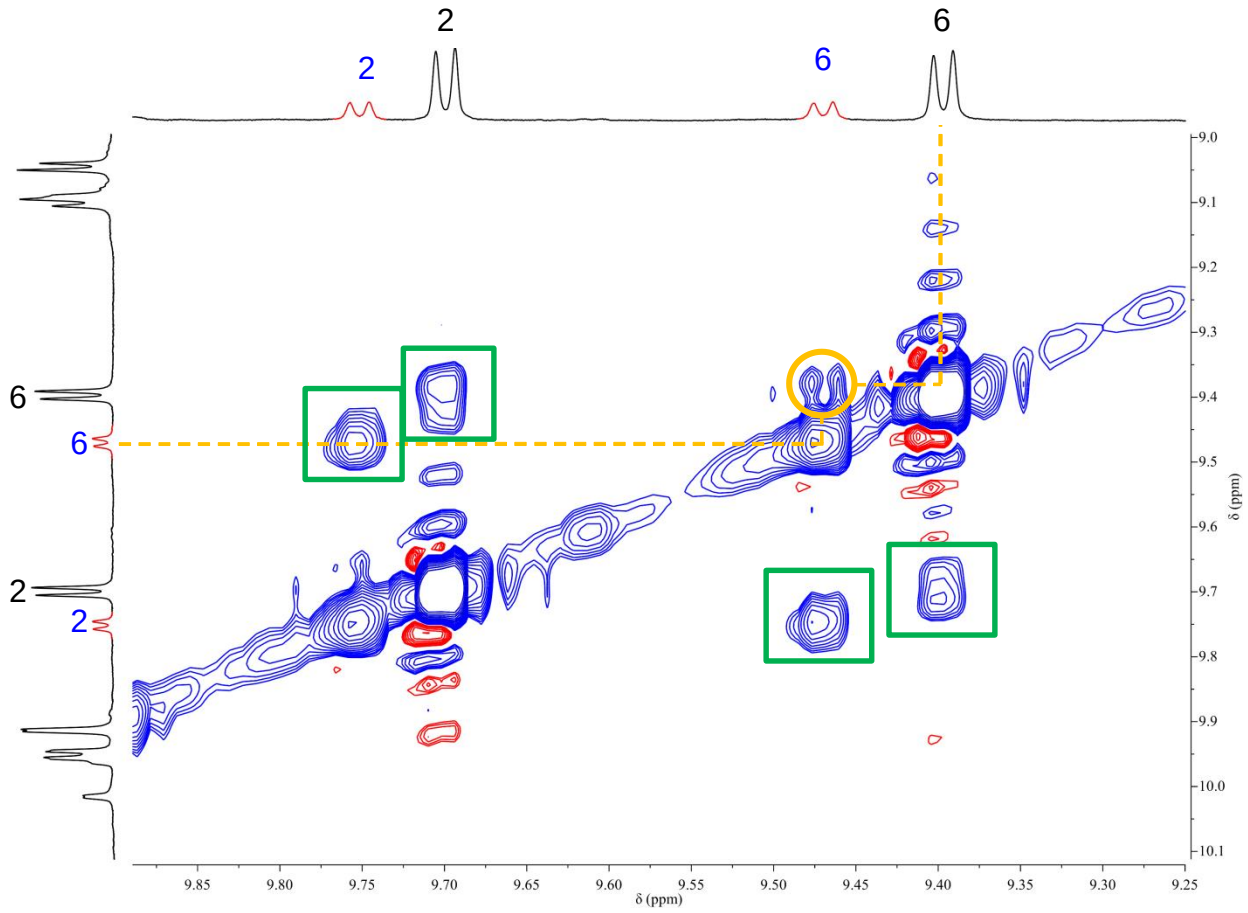

Figure S10. Enlargement of the ROESY NMR spectrum ($CDCl_3$, 50°C, mixing time = 200 ms) of the two stereoisomers of tape [{*t*,*c*,*c*-$RuCl_2(CO)_2$}$_4$(3′*cis*DPyMP)$_2$(4′TPyP)] (**D_3-T_4-D_3**). See Scheme S3 for the labeling scheme. The resonances of the minor isomer, presumably belonging to (**D_3-T_4-D_3**)$_Z$, are labeled in blue. The intermolecular exchange cross peak (blue) is evidenced with an orange frame. The intramolecular exchange cross peaks (blue), already visible in the room temperature spectrum of Figure S9, are in green frames.

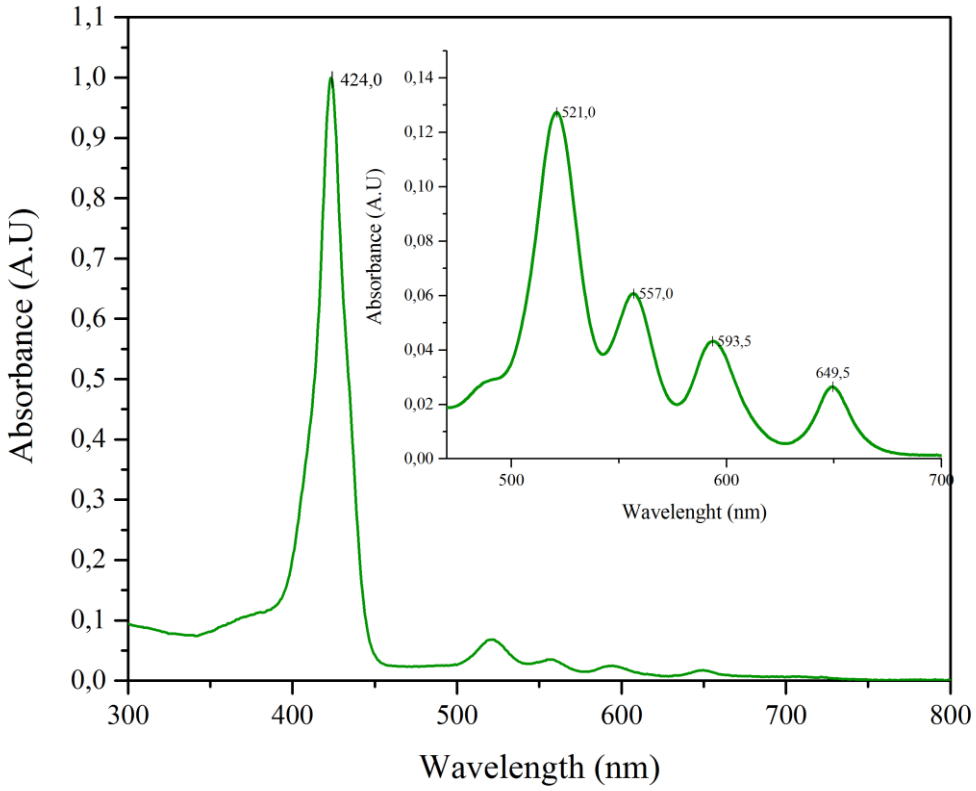

Figure S11. Normalized UV-Vis absorption spectrum ($CHCl_3$) of tape [{*t*,*c*,*c*-$RuCl_2(CO)_2$}$_4$(3′*cis*DPyMP)$_2$(4′TPyP)] (**D_3-T_4-D_3**).

Tape [{*t,c,c*-$RuCl_2(CO)_2$}$_4$(4′*cis*DPyMP)$_2$(3′TPyP)] (D_4-T_3-D_4) and [{*t,c,c*-$RuCl_2(CO)_2$}$_4$(Zn·4′*cis*DPyMP)$_2$(Zn·3′TPyP)] (ZnD_4-ZnT_3-ZnD_4).

The tri-porphyrin tape [{*t,c,c*-$RuCl_2(CO)_2$}$_4$(4′*cis*DPyMP)$_2$(3′TPyP)] (**D_4-T_3-D_4**) was obtained in acceptable yield by treatment of **5** with ca. 0.5 equiv. of 3′TPyP (Scheme S4) followed by chromatographic purifications.

Additional NMR characterization (Scheme S4 for the labeling scheme): The two sets of signals in the ^{1}H NMR spectrum have features similar to those of the 2+2 heteroleptic metallacycle [{*t,c,c*-$RuCl_2(CO)_2$}$_2$(4′*cis*DPyP)(3′TPyP)] (**1**) [46]: in the high frequency region the H2′ singlet and H6′ doublet of 3′TPyP are visible, whereas the H2 and H6 doublets of the two equivalent 4′*cis*DPyMP's fall at lower frequencies (between 9.2 and 9.7 ppm). Throughout the spectrum the fine structure of the resonances of the major isomer are well defined, whereas those of the minor isomer are less clear due to their low intensity and some overlapping. The H-H COSY and ROESY spectra allowed us to assign the resonances of the pyrrole protons of the major isomer: consistent with the symmetry of the compound, the βH protons of the two equivalent 4′*cis*DPyMP's give two singlets (Hβ1 and Hβ4) and two doublets (Hβ2 and Hβ3); these latter are connected in the COSY spectrum (Figure S12). In the ROESY spectrum (Figure S13) the doublet at 8.63 ppm shows NOE cross peaks with the multiplets of the *ortho* protons H*o* and H*o*′ (7.62 and 7.78 ppm, respectively, blue frame in the figure) and was thus assigned to Hβ3; on the other hand the resonance at 8.49 ppm was assigned to the overlapping doublet of Hβ2 and singlet of Hβ4 as it correlates (green frame) with the resonances of the *ortho* protons (close to Hβ4) and with that of H3 (close to Hβ2). Protons Hβ1 are those most affected by the shielding cone of the adjacent 3′TPyP and in fact their singlet is upfield shifted at 7.06 ppm; it has NOE cross peaks (orange frame) with the resonances at 7.87 and 8.95 ppm that were thus assigned to H5 and Hβ1′, respectively. The correlation between the Hβ1 singlet of 4′*cis*DPyMP and the Hβ1′ singlets of 3′TPyP is consistent with the distance of ca. 3.9 Å between the two protons found in the X-ray structure (see Figure S30).

The ROESY spectrum (Figure S13) also shows intramolecular exchange cross peaks between the H2 and H6 resonances (for both isomers) caused by the rotation of the pyridyl ring (Figure S14); however, no intermolecular exchange cross peaks between the two conformers are visible. This may be explained by assuming that the exchange between the two species is too slow with respect to the time scale of the NMR experiment (mixing time 100 ms). However, when the sample was dissolved in CD_2Cl_2 the relative abundance of the two isomers changed compared to $CDCl_3$ (Figure S15) suggesting that also in this case the two isomers are in slow conformational equilibrium. The H-H COSY spectrum in this solvent (Figure S16) shows the cross peaks between the resonances of

pyrrole protons (βH) and the singlets of the inner NH protons that confirm the attributions reported above.

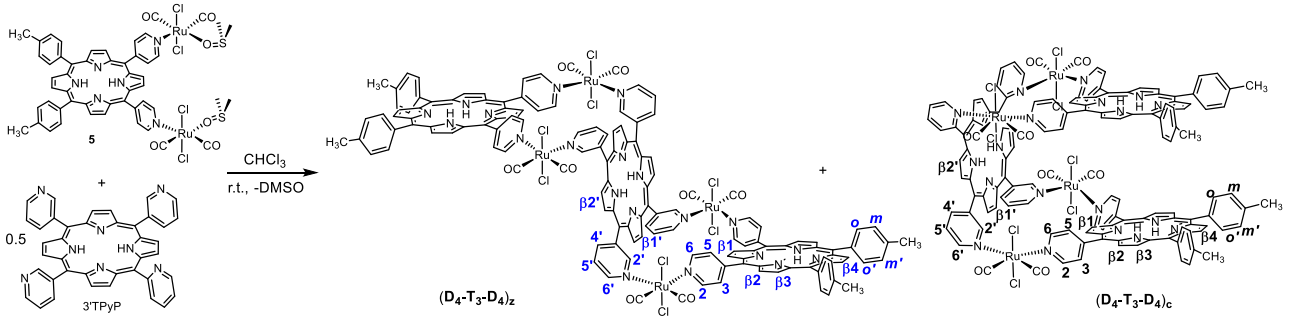

Scheme S4. The preparation of the two stereoisomers of tape [{*t*,*c*,*c*-$RuCl_2(CO)_2$}$_4$(4′*cis*DPyMP)$_2$(3′TPyP)] (**D_4-T_3-D_4**) with labeling scheme.

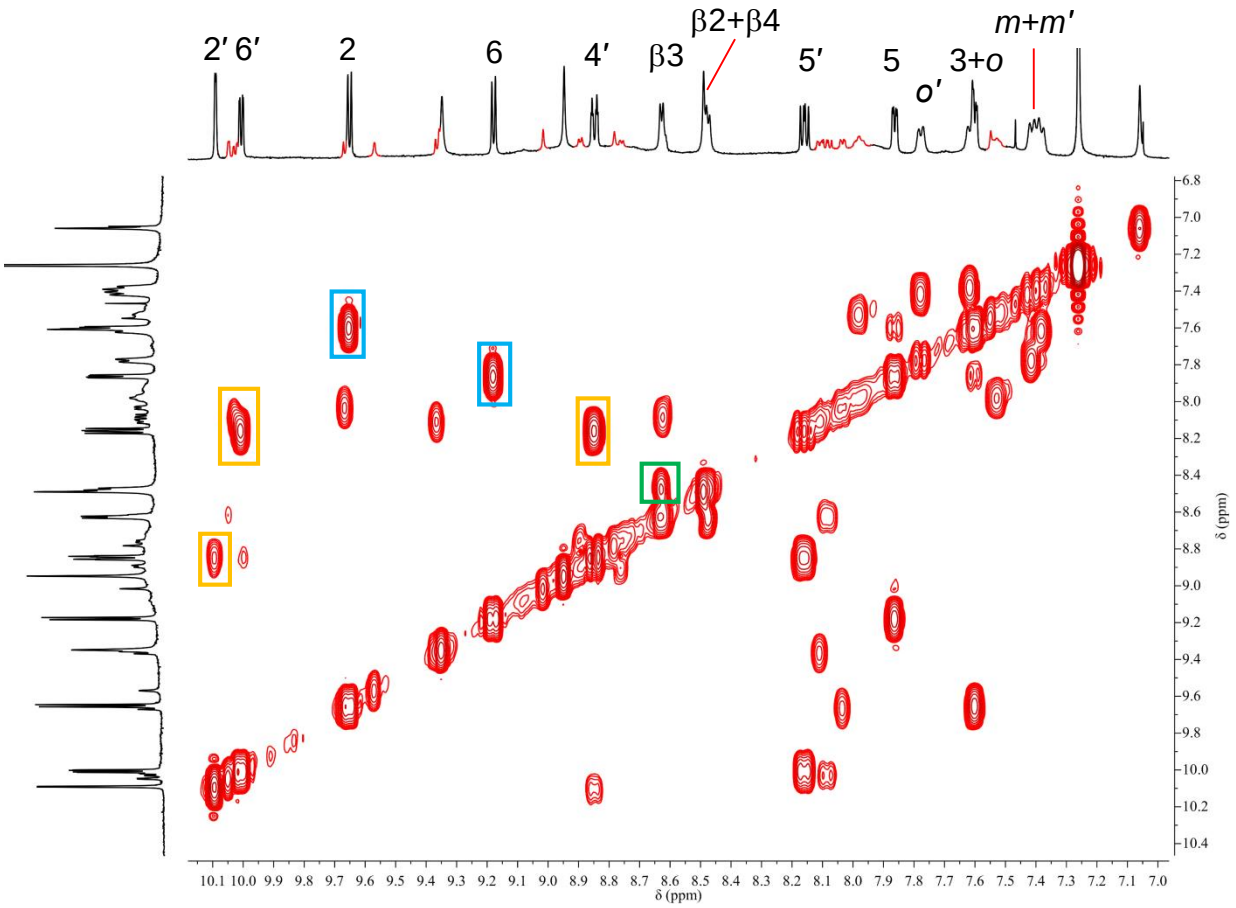

Figure S12. H-H COSY NMR spectrum (aromatic region, $CDCl_3$) of the two stereoisomers of tape [{*t*,*c*,*c*-$RuCl_2(CO)_2$}$_4$(4′*cis*DPyMP)$_2$(3′TPyP)] (**D_4-T_3-D_4**). Only selected resonances of the major isomer, presumably belonging to (**D_4-T_3-D_4**)$_z$, are labeled (see Scheme S4 for the labeling scheme). The resonances of the minor isomer are in red. Cross peaks connecting resonances of 3′-pyridyl ring protons (major species) are framed in orange, those of 4′-pyridyl ring protons in framed blue. The cross peak between the two doublets of the 4′*cis*DPyMP pyrrole protons Hβ2 and Hβ3 are in a green frame.

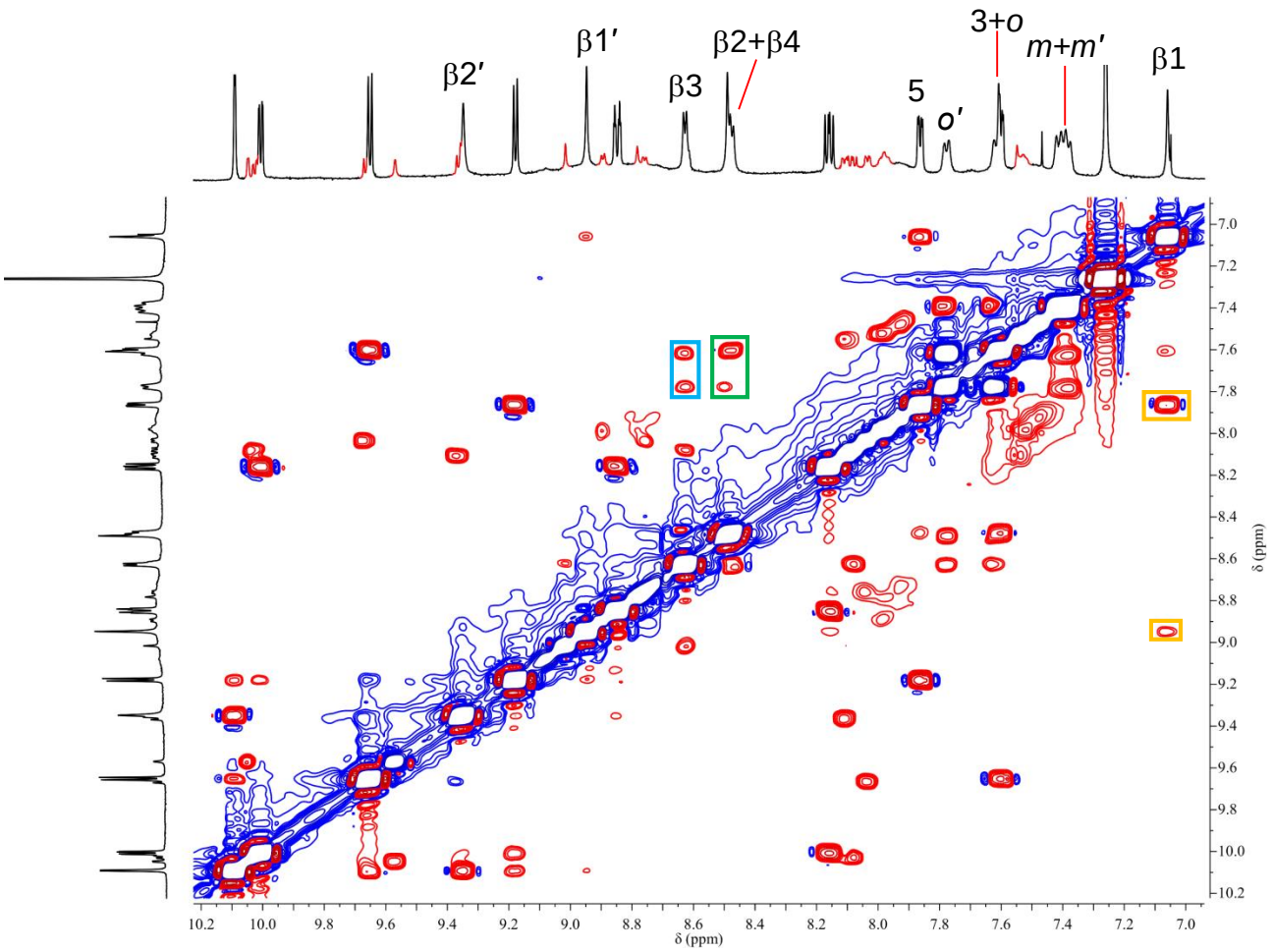

Figure S13. H-H ROESY NMR spectrum (aromatic region, $CDCl_3$) of the two stereoisomers of tape [{*t*,*c*,*c*-$RuCl_2(CO)_2$}$_4$(4′*cis*DPyMP)$_2$(3′TPyP)] (**D_4-T_3-D_4**). Only selected resonances of the major isomer, presumably belonging to (**D_4-T_3-D_4**)$_z$, are labeled (see Scheme S4 for the labeling scheme). Primed βH resonances belong to protons of 3′TPyP. The resonances of the minor isomer are in red. Cross peaks connecting resonances of 3′-pyridyl ring protons (major species) are framed in orange, those of 4′-pyridyl ring protons are framed in blue. The cross peak between the two doublets of the 4′*cis*DPyMP pyrrole protons Hβ2 and Hβ3 are in a green frame.

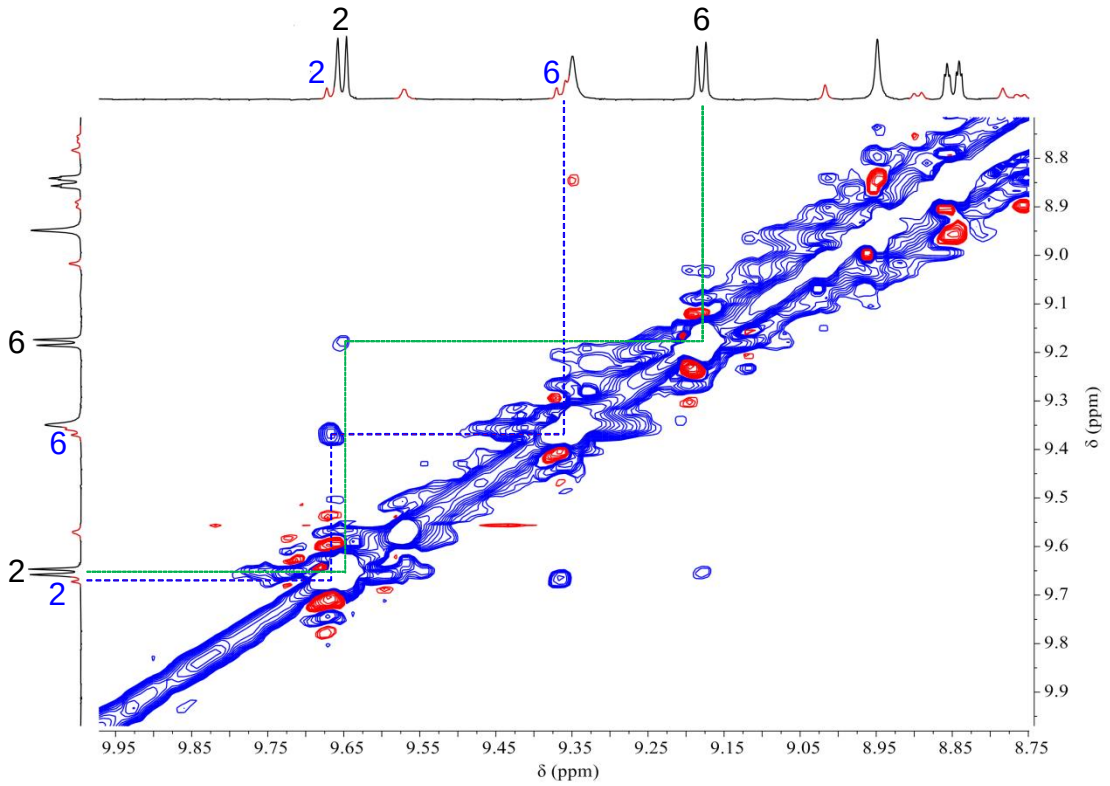

Figure S14. Enlargement of the H-H ROESY NMR spectrum (aromatic region, $CDCl_3$) of the two stereoisomers of tape [{*t*,*c*,*c*-$RuCl_2(CO)_2$}$_4$(4′*cis*DPyMP)$_2$(3′TPyP)] (**D$_4$-T$_3$-D$_4$**) showing the intramolecular exchange cross peaks between the H2 and H6 resonances (for both isomers) (see Scheme S4 for the labeling scheme). The resonances of the minor isomer (in red), presumably belonging to (**D$_4$-T$_3$-D$_4$**)$_z$, are labeled in blue.

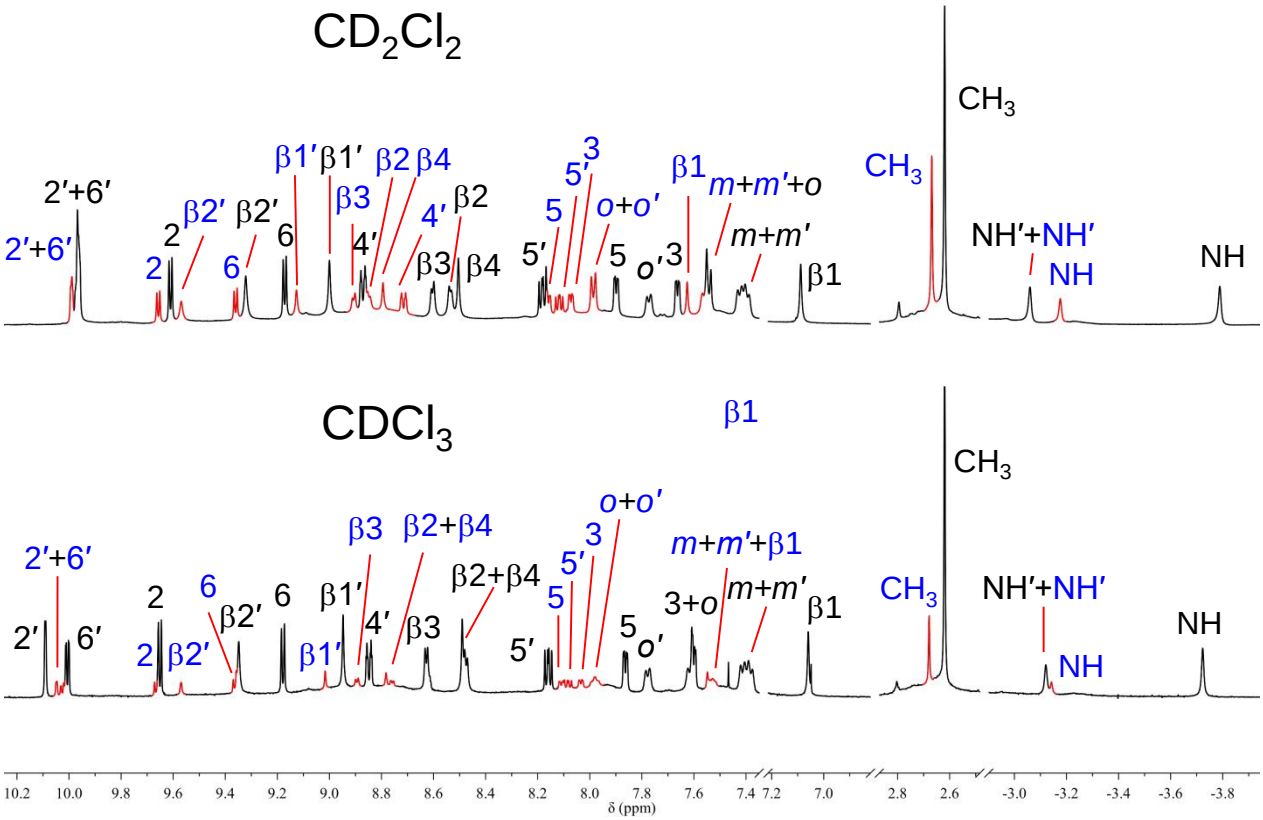

Figure S15. Comparison of the ^{1}H NMR spectra of the two stereoisomers of tape [{*t*,*c*,*c*-$RuCl_2(CO)_2$}$_4$(4′*cis*DPyMP)$_2$(3′TPyP)] (**D$_4$-T$_3$-D$_4$**) in $CDCl_3$ (bottom) and CD_2Cl_2 (top). See Scheme S4 for the labeling scheme. The resonances of the minor isomer (in red), presumably belonging to (**D$_4$-T$_3$-D$_4$**)$_z$, are labeled in blue. Primed βH and NH resonances belong to protons of 3′TPyP.

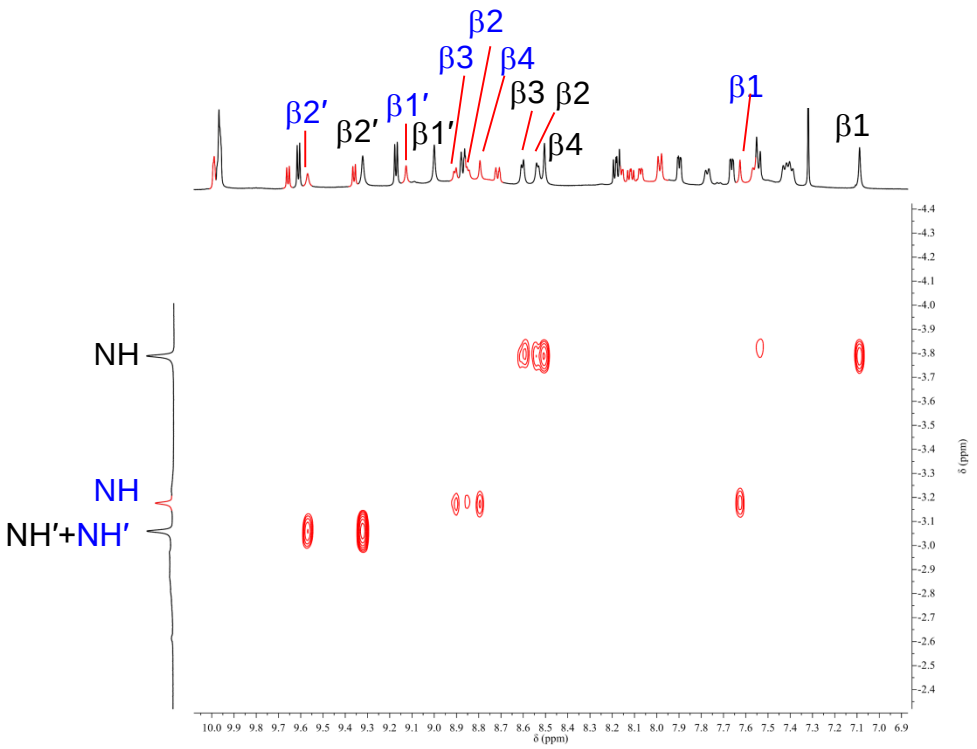

Figure S16. Enlargement of the H-H COSY NMR spectrum (CD_2Cl_2) of the two stereoisomers of tape [{*t*,*c*,*c*-$RuCl_2(CO)_2$}$_4$(4′*cis*DPyMP)$_2$(3′TPyP)] (**D_4-T_3-D_4**) showing the cross peaks between the resonances of pyrrole protons (βH for 4′*cis*DPyMP, βH′ for 3′TPyP) and inner NH protons: 4′*cis*DPyMP has four cross peaks with the NH singlets (visible also for the minor isomer), whereas 3′TPyP has two cross peaks with the NH′ singlets.

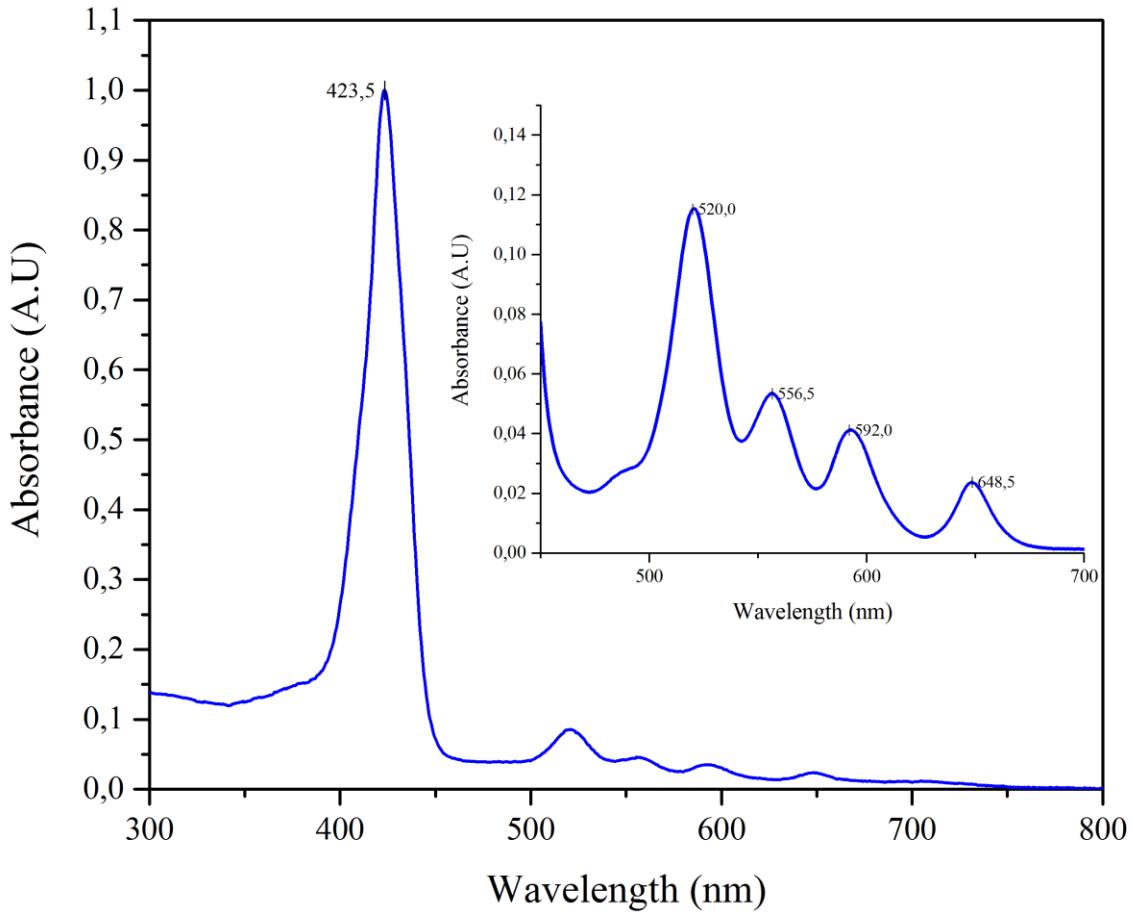

Figure S17. Normalized UV-Vis absorption spectrum ($CHCl_3$) of tape [{*t*,*c*,*c*-$RuCl_2(CO)_2$}$_4$(4′*cis*DPyMP)$_2$(3′TPyP)] (**D_4-T_3-D_4**).

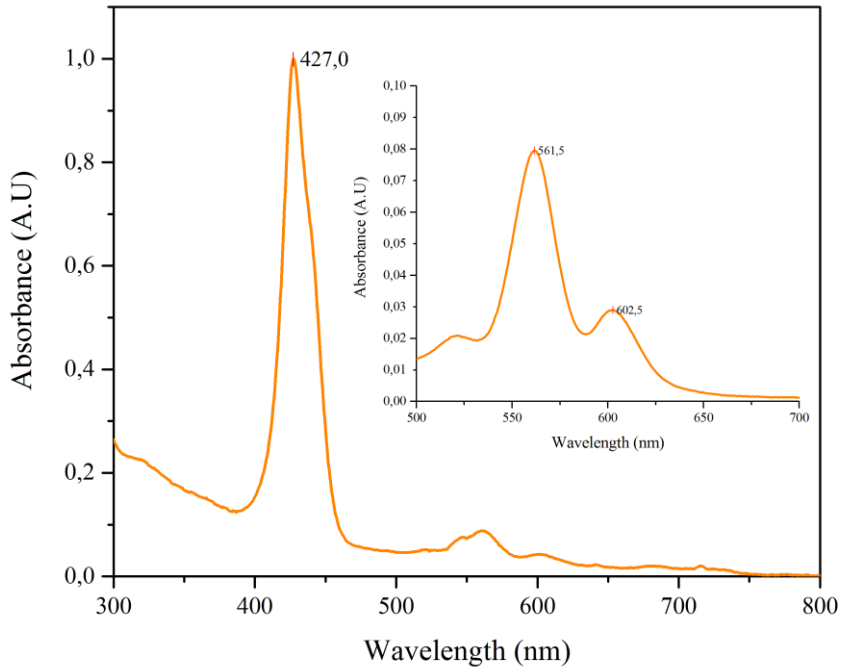

Figure S18. Normalized UV-Vis absorption spectrum ($CHCl_3$) of tape [{*t*,*c*,*c*-$RuCl_2(CO)_2$}$_4$(Zn·4′*cis*DPyMP)$_2$(Zn·3′TPyP)] (**ZnD_4-ZnT_3-ZnD_4**).

Tapes [{*t,c,c*-$RuCl_2(CO)_2$}$_4$(3′*cis*DPyMP)$_2$(3′TPyP)] (D_3-T_3-D_3) and [{*t,c,c*-$RuCl_2(CO)_2$}$_4$(Zn·3′*cis*DPyMP)$_2$(Zn·3′TPyP)] (ZnD_3-ZnT_3-ZnD_3).

The tri-porphyrin tape [{*t,c,c*-$RuCl_2(CO)_2$}$_4$(3′*cis*DPyMP)$_2$(3′TPyP)] (**D_3-T_3-D_3**) was obtained in acceptable yield by treatment of **4** with ca. 0.5 equiv. of 3′TPyP (Scheme S5) followed by chromatographic purifications.

Additional NMR characterization (Scheme S5 for the labeling scheme): The H-H COSY spectrum of [{*t,c,c*-$RuCl_2(CO)_2$}$_4$(3′*cis*DPyMP)$_2$(3′TPyP)] (**D_3-T_3-D_3**) (Figure S19), and the similarities with the spectrum of the homoleptic 2+2 metallacycle [{*t,c,c*-$RuCl_2(CO)_2$}$_2$(3′*cis*DPyP)$_2$] (**3**) [48], allowed us to identify some of the resonances of the 3′-pyridyl rings. As confirmed by the HSQC spectrum (Figure S20, the *o*C and *m*C ^{13}C resonances fall at ca. 145 and 128 ppm, respectively), the resonances of the tolyl protons fall in multiplets at ca. 8.10 ppm (*o*H) and 7.60 ppm (*m*H) that largely overlap with other resonances, thus preventing detailed assignments. According to integration, not all the resonances of the βH protons fall in the region between 9.20 and 8.80 ppm, but those of βH1 and βH1′ – as in the spectrum of **3** [48] – are likely to be upfield shifted by the shielding cone of the adjacent porphyrin and be in the broad peak centered at ca. 7.6 ppm (see below also the comments for the spectrum of **ZnD_3-ZnT_3-ZnD_3**). Besides the NH resonances (see text) it has been possible to assign unambiguously only the resonances of the pyridyl protons H2′ of both isomers. In the H-H COSY spectrum, the βH peak at 9.24 ppm has a cross peak with the NH singlet at –3.24 ppm (insert in Figure S20), thus the two protons belong to the same porphyrin, i.e. (based on NH integration and chemical shift considerations) to 3′TPyP of the major isomer. Saturation of the singlet at 10.10 ppm (belonging to an H2′ of the major species) gives an NOE enhancement with the βH peak at 9.24 ppm: thus, both protons belong to 3′TPyP and the peak at 10.10 ppm was assigned to H2′ of 3′TPyP (as a consequence, the singlet at 9.82 ppm was assigned to H2′ on the pyridyl rings of the external 3′*cis*DPyP's). Finally, in the ROESY spectrum (Figure S21) the H2′ singlet at 10.10 ppm has an exchange cross peak with that at 9.87, that thus was assigned to H2′ of 3′TPyP of the minor species.

The treatment of tape **D_3-T_3-D_3** with excess zinc acetate afforded the fully zincated product [{*t,c,c*-$RuCl_2(CO)_2$}$_4$(Zn·3′*cis*DPyMP)$_2$(Zn·3′TPyP)] (**ZnD_3-ZnT_3-ZnD_3**) in excellent yield (see below). The ^{1}H NMR spectrum of **ZnD_3-ZnT_3-ZnD_3** in $CDCl_3$ (Figure S22) is similar to that of the parent compound (except for the absence of the NH resonances and for the ca. 1:1 ratio between the isomers) but has sharper and better resolved peaks that allowed us to detect clearly between 7.8 and 7.9 ppm some βH resonances that in the spectrum of **D_3-T_3-D_3** overlap with H4 and H*o* multiplets. As already observed for the NMR spectra of **3** [48], such low-field pyrrole resonances (the others

occur between 8.9 and 9.3 ppm) belong to the eight βH protons – four on the central Zn·3′TPyP (βH1′) and four on the peripheral Zn·3′*cis*DPyMPs (βH1) – closer to the adjacent porphyrin and that feel its shielding effect.

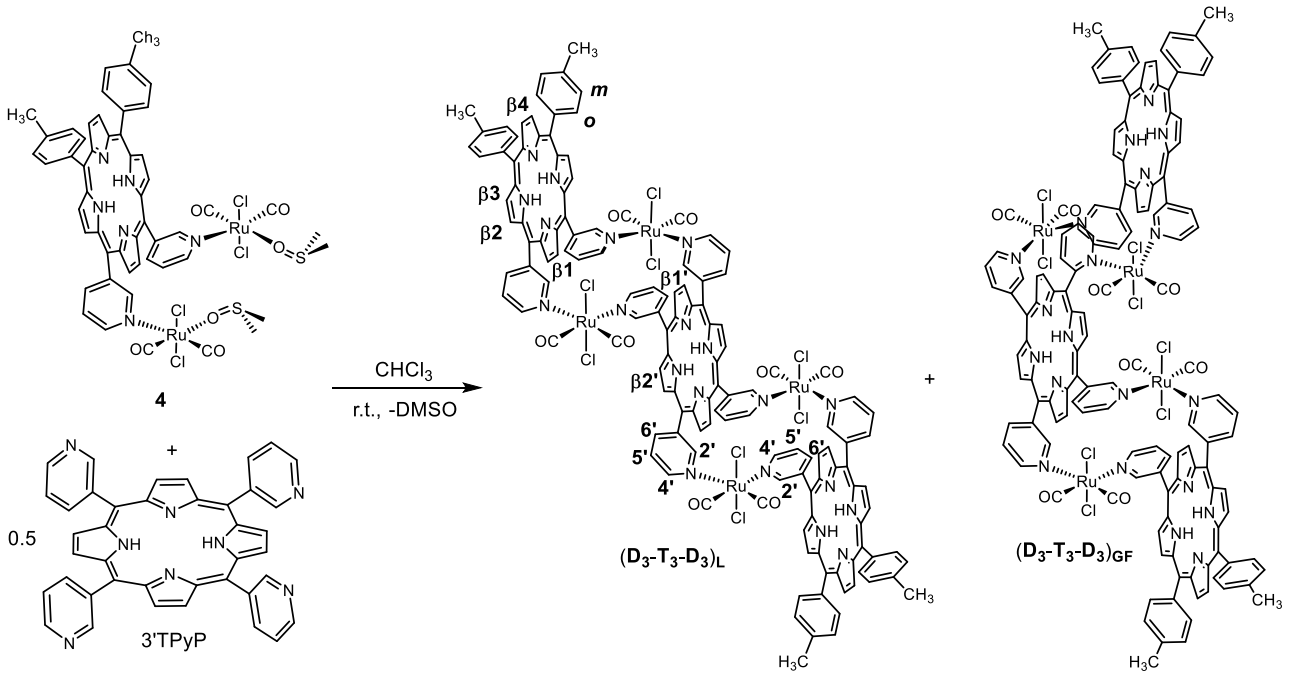

Scheme S5. The preparation of the two stereoisomers of tape [{*t*,*c*,*c*-$RuCl_2(CO)_2$}$_4$(3′*cis*DPyMP)$_2$(3′TPyP)] (**D_3-T_3-D_3**) with labeling scheme.

Preparation of [{*t*,*c*,*c*-$RuCl_2(CO)_2$}$_4$(Zn·3′*cis*DPyMP)$_2$(Zn·3′TPyP)] (ZnD_3-ZnT_3-ZnD_3). To a 40.0 mg amount of **D_3-T_3-D_3** (0.0145 mmol) dissolved in 45 mL of $CHCl_3$ a 12.8 mg amount of $Zn(AcO)_2{\cdot}2H_2O$ (0.06 mmol, ca. 4 equiv.) dissolved in 1 mL of MeOH was added. The solution was stirred at room temperature in the dark for 22 h and then washed with water (3 × 70 mL). The organic phase was dried on Na_2SO_4, the solvent was removed under reduced pressure and the solid dried under vacuum. Yield 29.3 mg (67%). $C_{136}H_{84}N_{20}Cl_8O_8Ru_4Zn_3$, M_w = 3010.32. ^{1}H NMR ($CDCl_3$), low-case m and M stand for minor and major stereoisomer, respectively; primed βH labels belong to the central 3′TPyP (see also Scheme S5 for the numbering scheme), δ (ppm): 10.04–9.82 (4 s, $8H_M$+$8H_m$, $2'_M$+$2'_m$), 9.72–9.48 (3 d, $8H_M$+$8H_m$, $6'_M$+$6'_m$), 9.34–8.81 (singlets + doublets, $16H_M$+$16H_m$, β2-4_M+β2′$_M$+β2-4_m+β2′$_m$), 8.25–7.95 (m, $16H_M$+$16H_m$, $4'_M$+$4'_m$+o_M+o_m), 7.93–7.75 (s+m, $8H_M$+$8H_m$, β1$_M$+β1′$_M$+β1$_m$+β1′$_m$), 7.55 (m, $16H_M$+$16H_m$, $5'_M$+$5'_m$+m_M+m_m), 2.75 (s, $12H_m$, Me_m), 2.74 (s, $12H_M$, Me_M). UV–vis [$CHCl_3$; λ_{max} (nm), (ε × 10^4 (cm^{-1} M^{-1})]: 426(58.4, Soret band), 438.5 (42.6, Soret band), 560.5 (4.53), 600(1.55). IR (selected bands in $CHCl_3$, cm^{-1}): 2074 (ν*C*O), 2014 (ν*C*O).

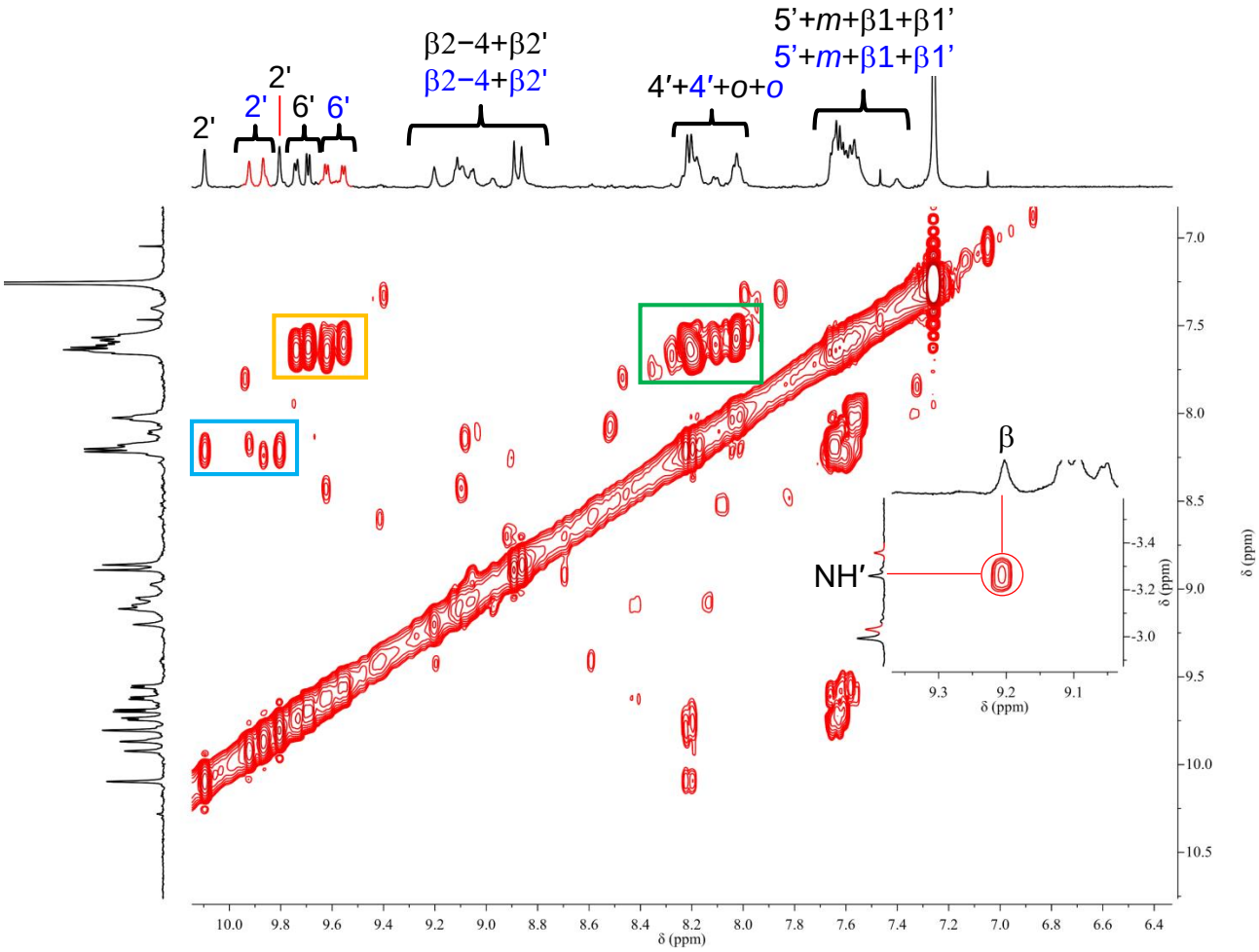

Figure S19. H-H COSY NMR spectrum (aromatic region, $CDCl_3$) of the two stereoisomers of tape [{*t*,*c*,*c*-$RuCl_2(CO)_2$}$_4$(3′*cis*DPyMP)$_2$(3′TPyP)] (**D_3-T_3-D_3**) (see Scheme S5 for the labeling scheme). Primed βH and NH resonances belong to protons of 3′TPyP. The resonances of the minor isomer (in red) are labeled in blue. Cross peaks between H2′ and the corresponding H4′ resonances are framed in blue, those between H4′ and H5′ in green, and those between H5′ and H6′ in orange.

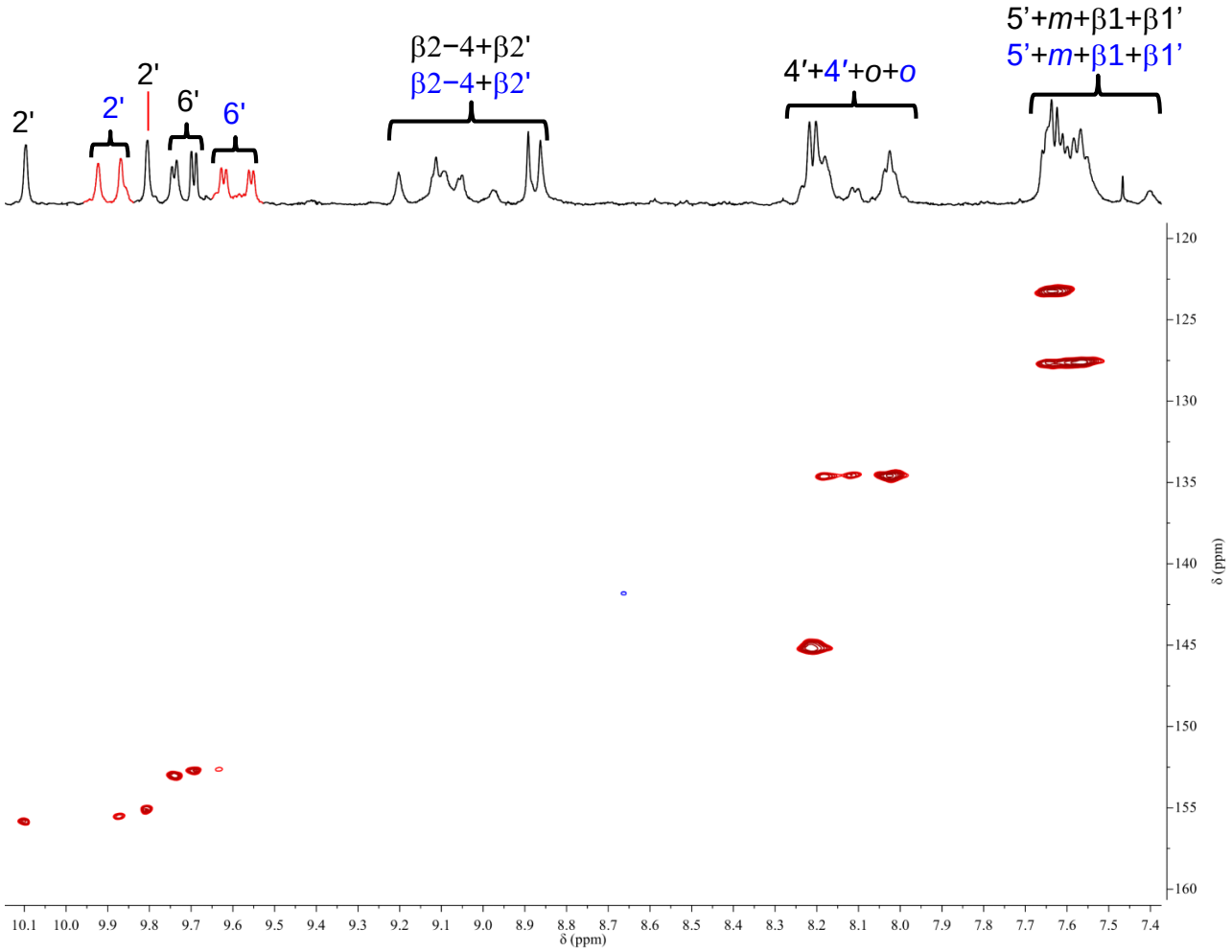

Figure S20. HSQC NMR spectrum ($CDCl_3$) of the two stereoisomers of tape [{*t*,*c*,*c*-$RuCl_2(CO)_2$}$_4$(3′*cis*DPyMP)$_2$(3′TPyP)] (**D_3-T_3-D_3**). For labeling scheme see Scheme S5. Primed βH resonances belong to protons of 3′TPyP. The resonances of the minor isomer (in red) are labeled in blue. Quite often, the pyrrole protons give very weak cross peaks in the HSQC spectra, not visible in normal plots.

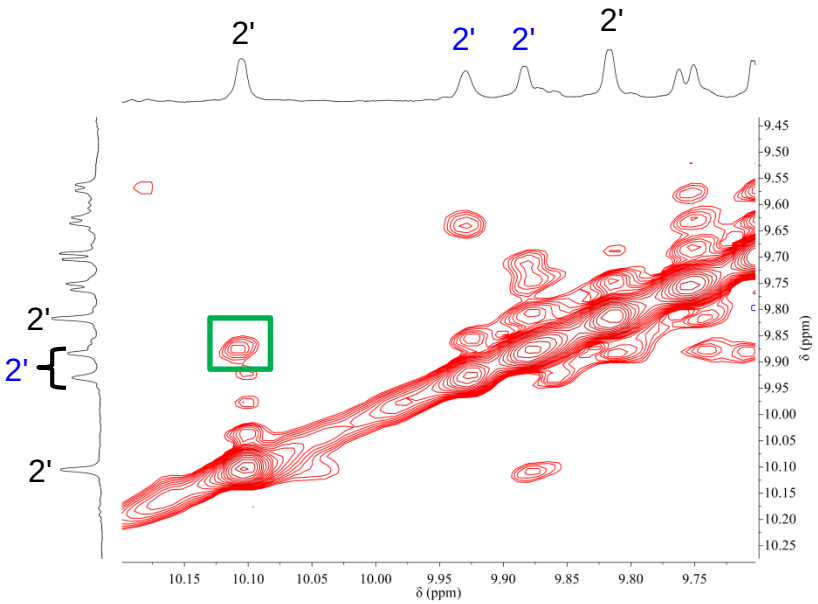

Figure S21. Enlargement of the H-H ROESY NMR spectrum ($CDCl_3$) of the two stereoisomers of tape [{*t*,*c*,*c*-$RuCl_2(CO)_2$}$_4$(3′*cis*DPyMP)$_2$(3′TPyP)] (**D_3-T_3-D_3**) showing the exchange cross peak (green frame) that connects the H2′ singlets of the two stereoisomers. For labeling scheme see Scheme S5. The resonances of the minor isomer (in red) are labeled in blue.

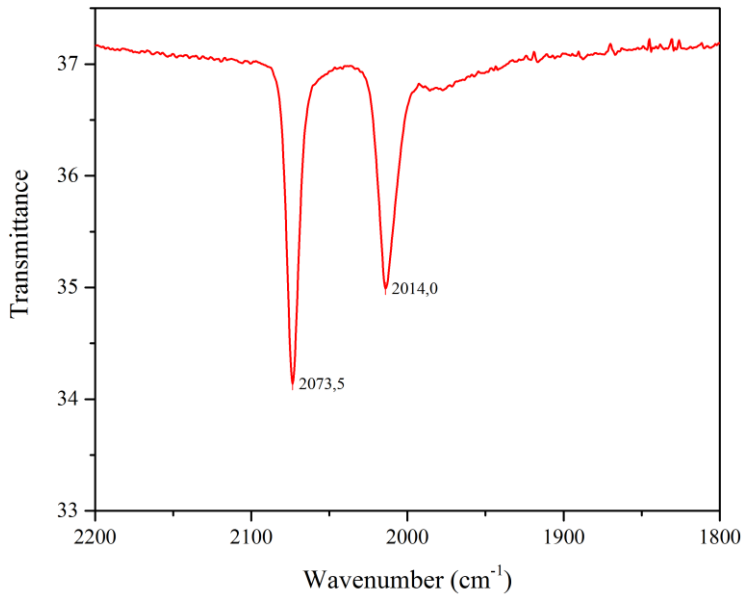

Figure S22. CO stretching region in the IR spectrum ($CHCl_3$) of tape [{*t*,*c*,*c*-$RuCl_2(CO)_2$}$_4$(3′*cis*DPyMP)$_2$(3′TPyP)] (**D_3-T_3-D_3**).

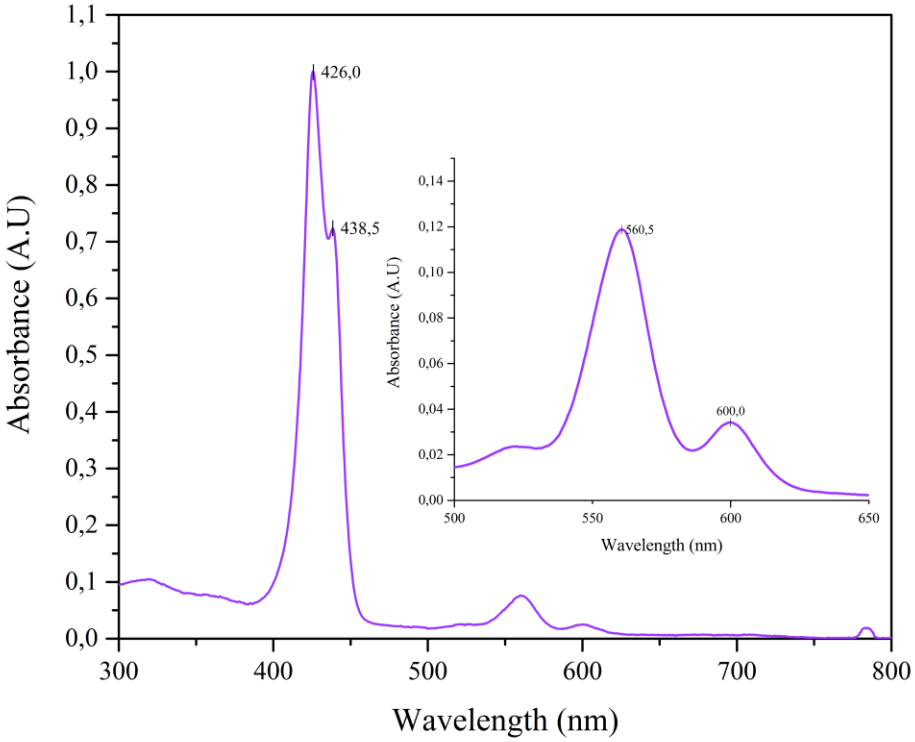

Figure S23. Normalized UV-Vis absorption spectrum ($CHCl_3$) of tape [{*t*,*c*,*c*-$RuCl_2(CO)_2$}$_4$(Zn·3′*cis*DPyMP)$_2$(Zn·3′TPyP)] (**ZnD_3-ZnT_3-ZnD_3**).

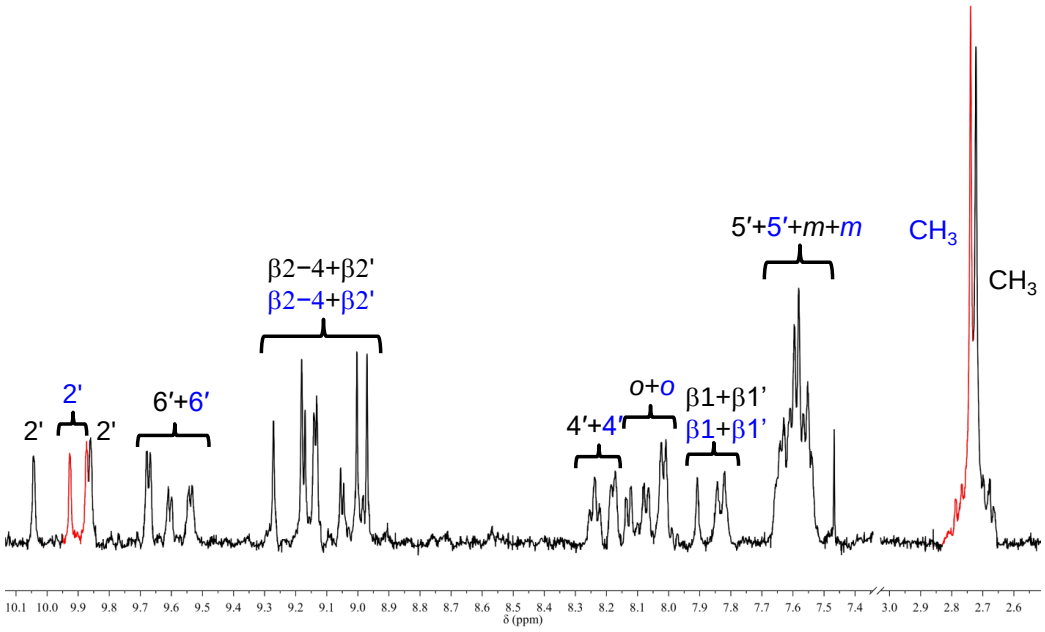

Figure S24. ^{1}H NMR spectrum ($CDCl_3$) of the two stereoisomers of tape [{*t*,*c*,*c*-$RuCl_2(CO)_2$}$_4$(Zn·3′*cis*DPyMP)$_2$(Zn·3′TPyP)] (**ZnD$_3$-ZnT$_3$-ZnD$_3$**). For labeling scheme see Scheme S5. Primed βH resonances belong to protons of 3′TPyP. The (identified) resonances of the minor isomer (in red) are labeled in blue.

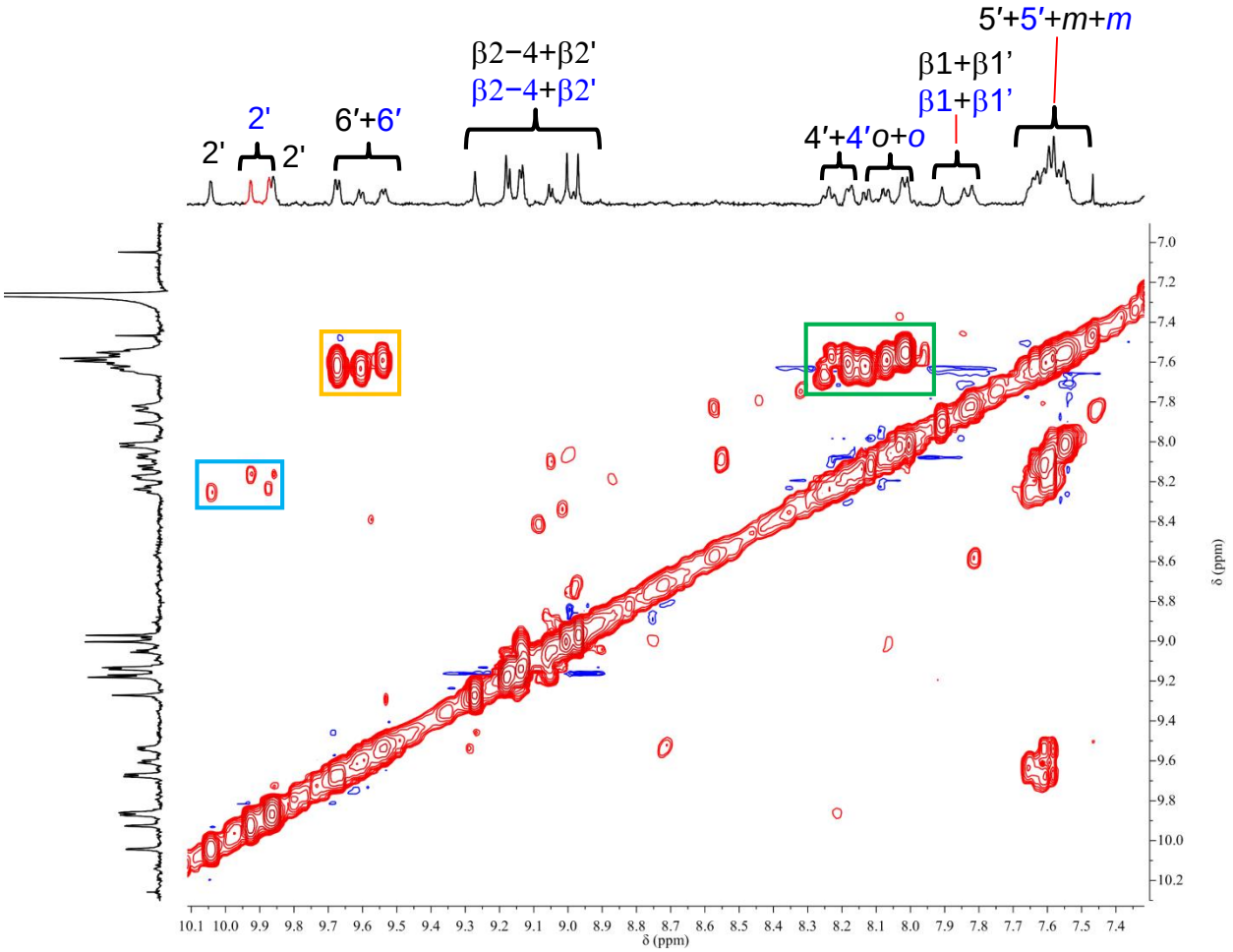

Figure S25. H-H COSY NMR spectrum (aromatic region, $CDCl_3$) of the two stereoisomers of tape [{*t*,*c*,*c*-$RuCl_2(CO)_2$}$_4$(Zn·3′*cis*DPyMP)$_2$(Zn·3′TPyP)] (**ZnD_3-ZnT_3-ZnD_3**). For labeling scheme see Scheme S5. Primed βH resonances belong to protons of 3′TPyP. The (identified) resonances of the minor isomer (in red) are labeled in blue. Cross peaks between H2′ and the corresponding H4′ resonances are framed in pale blue, those between H4′ and H5′ in green, and those between H5′ and H6′ in orange.

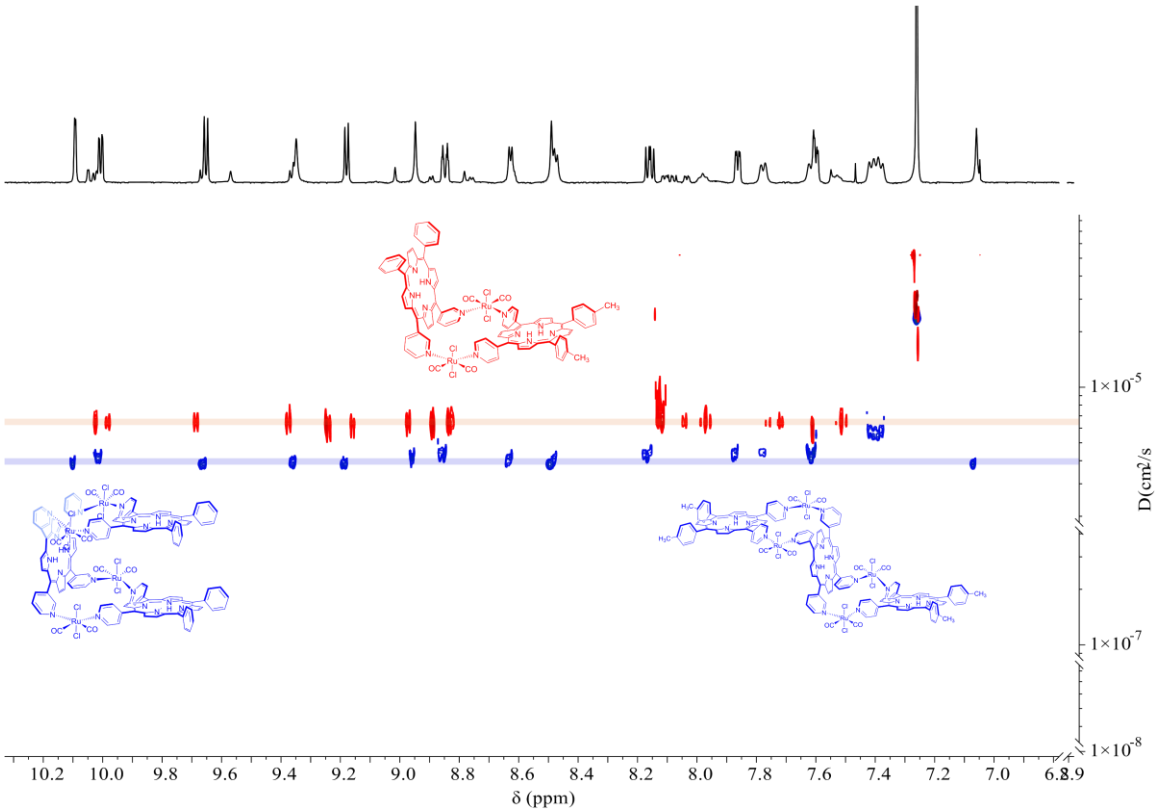

Figure S26. Bidimensional DOSY spectrum ($CDCl_3$) of [{*t*,*c*,*c*-$RuCl_2(CO)_2$}$_4$(4′*cis*DPyMP)$_2$(3′TPyP)] (**D_4-T_3-D_4**) (blue) compared with that of the 2+2 metallacycle [{*t*,*c*,*c*-$RuCl_2(CO)_2$}$_2$(4′*cis*DPyP)(3′*cis*DPyP)] (**1**) (red).

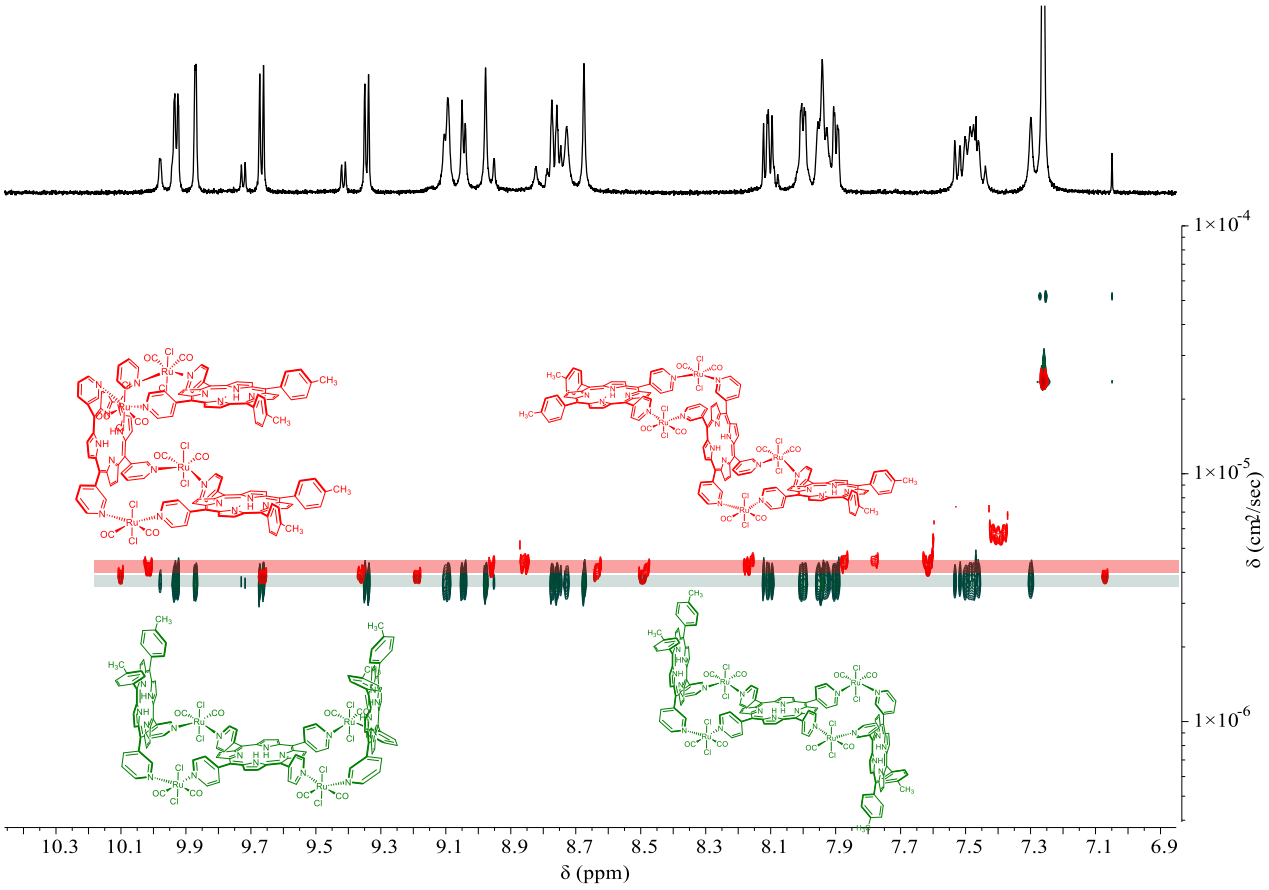

Figure S27. Bidimensional DOSY spectrum ($CDCl_3$) of [{*t*,*c*,*c*-$RuCl_2(CO)_2$}$_4$(3′*cis*DPyMP)$_2$(4′TPyP)] (**D_3-T_4-D_3**) (green) compared with that of [{*t*,*c*,*c*-$RuCl_2(CO)_2$}$_4$(4′*cis*DPyMP)$_2$(3′TPyP)] (**D_4-T_3-D_4**) (red).

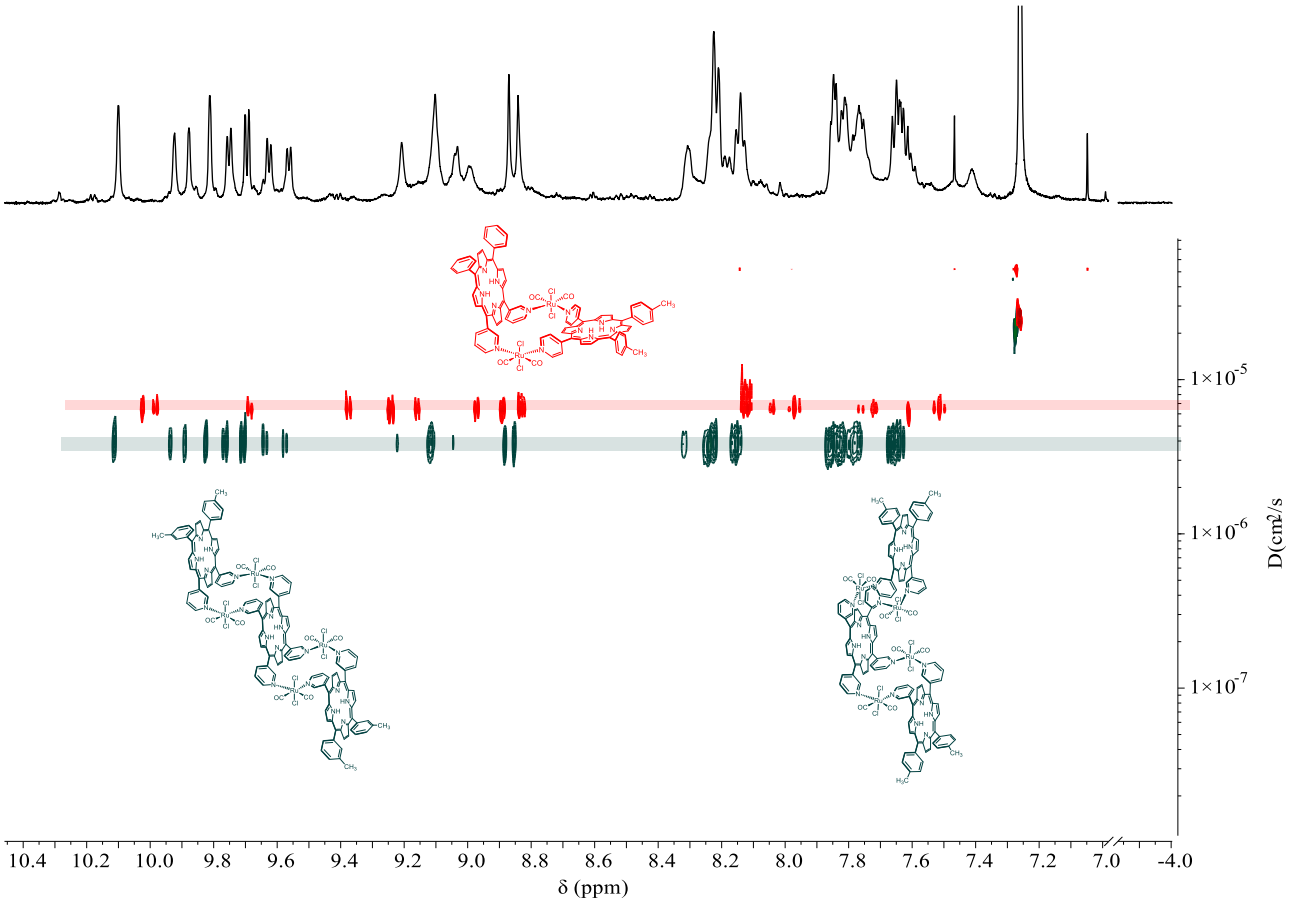

Figure S28. Bidimensional DOSY spectrum ($CDCl_3$) of [{*t*,*c*,*c*-$RuCl_2(CO)_2$}$_4$(3′*cis*DPyMP)$_2$(3′TPyP)] (**D_3-T_3-D_3**) (green) compared with that of the 2+2 metallacycle [{*t*,*c*,*c*-$RuCl_2(CO)_2$}$_2$(4′*cis*DPyP)(3′*cis*DPyP)] (**1**) (red).

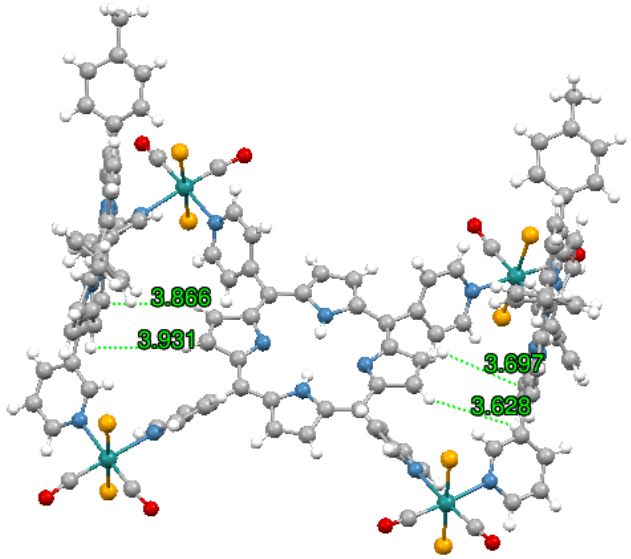

Figure S29. The X-ray molecular structure of stereoisomer $(\mathbf{D_3\text{-}T_4\text{-}D_3})_C$ showing the distances between protons β1′ on 4′TPyP and β1 on the adjacent 3′*cis*DPyMP's. Color code: N = blue, Cl = yellow, O = red.

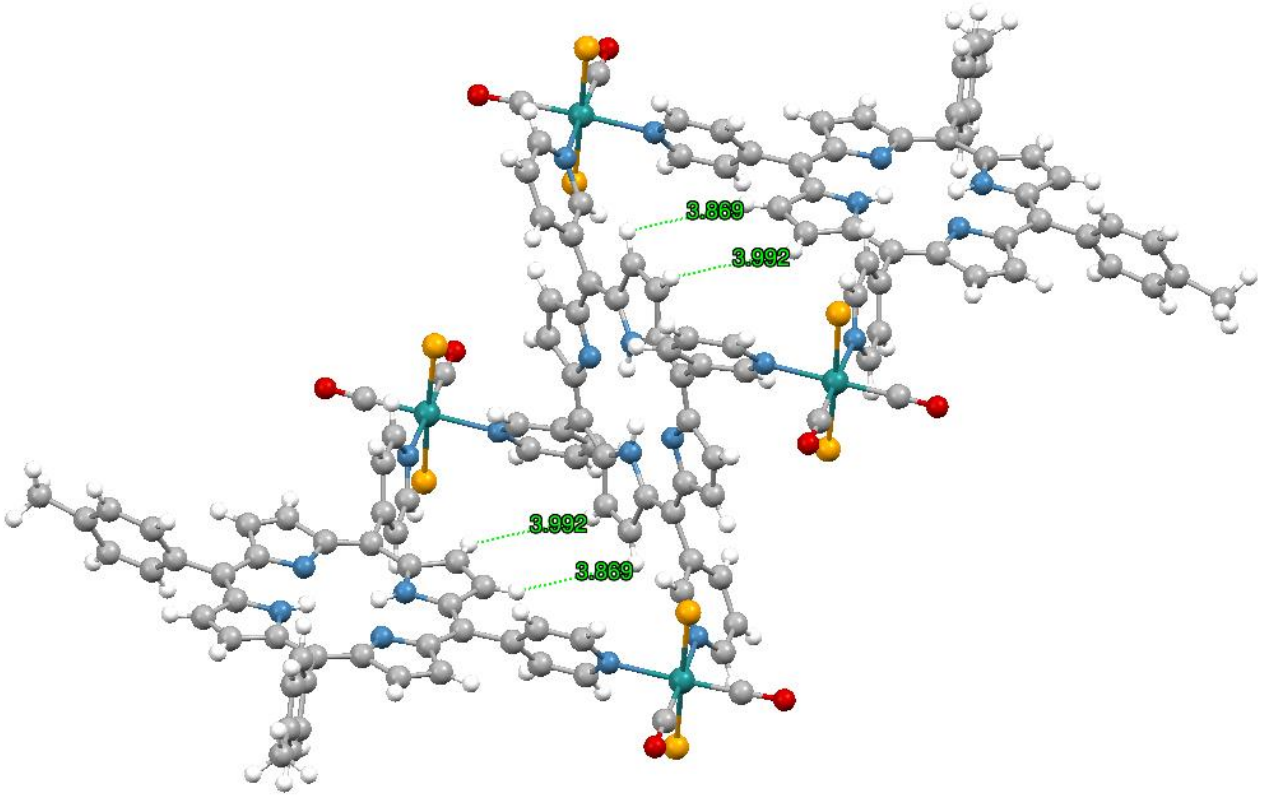

Figure S30. The X-ray molecular structure of stereoisomer $(\mathbf{D_4\text{-}T_3\text{-}D_4})_z$ showing the distances between protons β1′ on 3′TPyP and β1 on the adjacent 4′*cis*DPyMP's. Color code: N = blue, Cl = yellow, O = red.

Table S1. Crystallographic data and refinement details for compounds $(\mathbf{D_3\text{-}T_4\text{-}D_3})_C$ and $(\mathbf{D_4\text{-}T_3\text{-}D_4})_z$.

	$(\mathbf{D_3\text{-}T_4\text{-}D_3})_C$	$(\mathbf{D_4\text{-}T_3\text{-}D_4})_z$
Empirical Formula	$C_{136}H_{90}N_{20}Cl_8O_8Ru_4 \cdot 2.4CHCl_3 \cdot 0.4H_2O$	$C_{136}H_{90}N_{20}Cl_8O_8Ru_4 \cdot 4C_6H_{14} \cdot 0.3H_2O$
Formula weight (Da)	3113.84	3170.24
Temperature (K)	100(2)	100(2)
Wavelength (Å)	0.700	0.700
Crystal system	triclinic	triclinic
Space Group	P –1	P –1
a (Å)	16.75(2)	15.11(2)
b (Å)	23.10(2)	17.406(5)
c (Å)	24.98(2)	18.944(11)
α (°)	72.47(3)	92.38(2)
β (°)	73.27(5)	117.05(6)
γ (°)	80.69(3)	109.95(2)
V ($Å^3$)	8796(16)	4054(6)
Z	2	1
ρ ($g \cdot cm^{-3}$)	1.176	1.299
F(000)	3130	1625
μ (mm^{-1})	0.585	0.528
θ min, max (°)	0.871, 16.958	1.223, 22.884
Resolution (Å)	1.20	0.90
Total refl. collctd	44653	71126
Independent refl.	10259	11160
Obs. Refl. [Fo>4σ(Fo)]	4357	5455
I/σ(I) (all data)	3.09	7.34
I/σ(I) (max res)	1.28	1.15
Completeness (all data)	0.963	0.960
R_{merge} (all data)	30.8%	14.2%
R_{merge} (max res)	977.4%	216.4%
Multiplicity (all data)	4.3	6.4
Multiplicity (max res)	4.5	6.2
Data/restraint/parameters	10259/1404/1745	11160/172/907
GooF	1.073	1.295
R[I>2.0σ(I)], wR2 [I>2.0σ(I)]	0.1252, 0.3104	0.1308, 0.3312
R (all data), wR2 (all data)	0.2148, 0.3896	0.2271, 0.4012

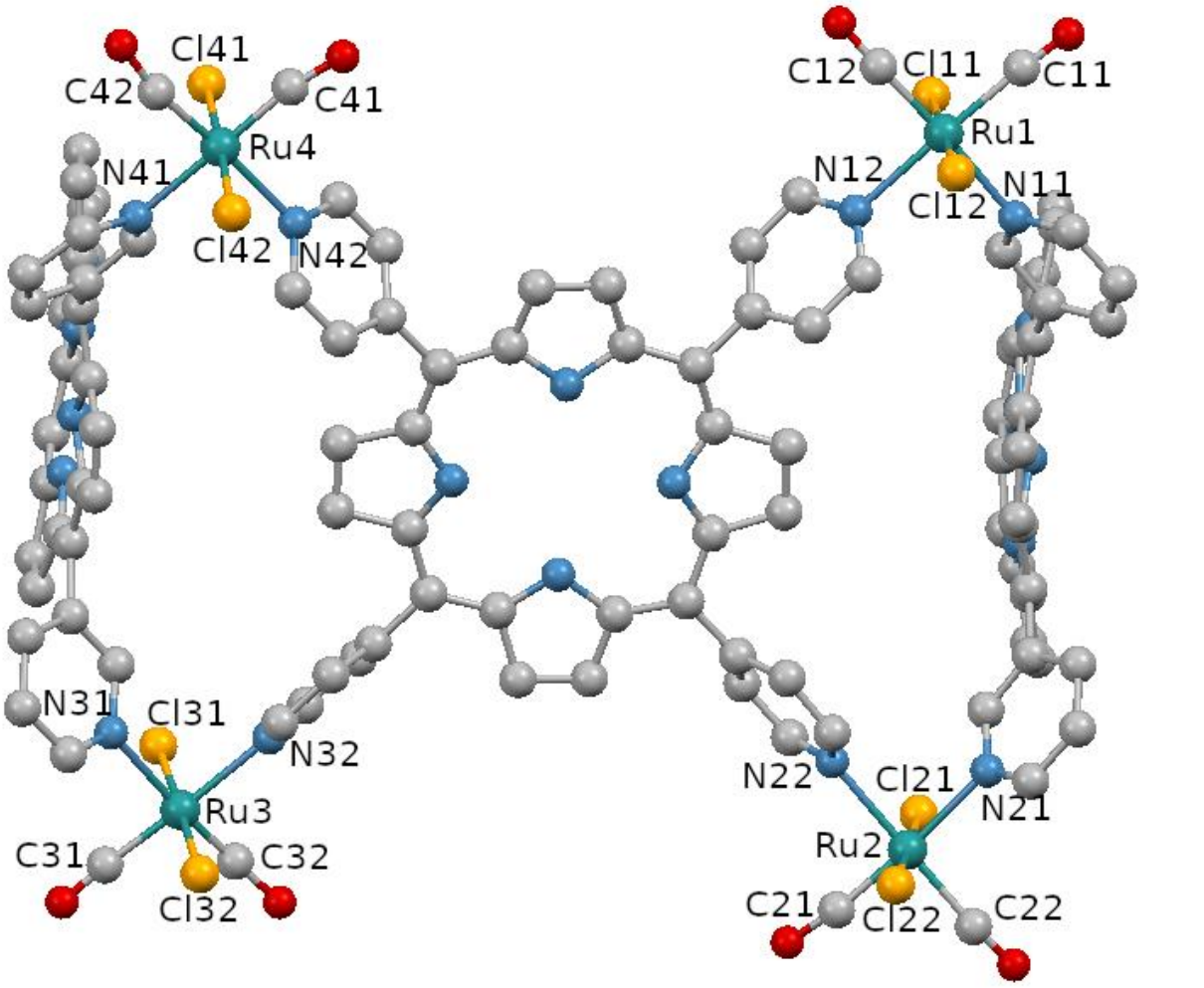

Figure S31. The X-ray molecular structure of stereoisomer $(\mathbf{D_3\text{-}T_4\text{-}D_3})_C$ (front view) with numbering scheme. The *meso*-tolyl groups on the two 3′*cis*DPyMP's and the hydrogen atoms have been omitted for clarity.

Table S2. Selected coordination distances (Å) and angles (°) for $(\mathbf{D_3\text{-}T_4\text{-}D_3})_C$ (see Figure S31).

Selected distances (Å)	
Ru1–C11	1.93(4)
Ru1–C12	1.84(3)
Ru1–Cl11	2.36(1)
Ru1–Cl12	2.36(1)
Ru1–N11	2.201(9)
Ru1–N12	2.252(7)
Ru2–C21	1.800(3)
Ru2–C22	1.94(3)
Ru2–Cl21	2.35(1)
Ru2–Cl22	2.36(1)
Ru2–N21	2.182(9)
Ru2–N22	2.236(6)
Ru3–C31	1.82(4)
Ru3–C32	1.63(4)
Ru3–Cl31	2.37(1)
Ru3–Cl32	2.35(1)
Ru3–N31	2.21(1)
Ru3–N32	2.226(7)
Ru4–C41	1.799(3)
Ru4–C42	1.84(3)
Ru4–Cl41	2.387(9)
Ru4–Cl42	2.35(1)
Ru4–N41	2.19(1)
Ru4–N42	2.246(6)

Selected angles (°)	
C11–Ru1–Cl11	87(1)
C11–Ru1–Cl12	94(1)
C11–Ru1–N11	91(1)
C11–Ru1–N12	175(1)
C12–Ru1–C11	93(2)
C12–Ru1–Cl11	90(1)
C12–Ru1–Cl12	91(1)
C12–Ru1–N11	176(1)
C12–Ru1–N12	90(1)
Cl11–Ru1–Cl12	178.9(3)
N11–Ru1–Cl11	88.5(4)

N11–Ru1–Cl12 90.8(4)
N11–Ru1–N12 86.1(6)
N12–Ru1–Cl11 89.0(5)
N12–Ru1–Cl12 90.1(4)
C21–Ru2–C22 89(1)
C21–Ru2–Cl21 93(1)
C21–Ru2–Cl22 87(1)
C21–Ru2–N21 176(1)
C21–Ru2–N22 92(1)
C22–Ru2–Cl21 91(1)
C22–Ru2–Cl22 89(1)
C22–Ru2–N21 96(1)
C22–Ru2–N22 179(2)
Cl21–Ru2–Cl22 179.8(3)
N21–Ru2–Cl21 87.2(4)
N21–Ru2–Cl22 92.8(5)
N21–Ru2–N22 83.7(6)
N22–Ru2–Cl21 90.5(5)
N22–Ru2–Cl22 89.4(5)
C31–Ru3–Cl31 88(1)
C31–Ru3–Cl32 91(1)
C31–Ru3–N31 91(1)
C31–Ru3–N32 177(1)
C32–Ru3–C31 93(2)
C32–Ru3–Cl31 91(1)
C32–Ru3–Cl32 90(1)
C32–Ru3–N31 176(1)
C32–Ru3–N32 90(1)
Cl32–Ru3–Cl31 178.7(3)
N31–Ru3–Cl31 87.1(4)
N31–Ru3–Cl32 92.5(5)
N31–Ru3–N32 86.4(6)
N32–Ru3–Cl31 90.6(4)
N32–Ru3–Cl32 90.6(5)
C41–Ru4–C42 90(1)
C41–Ru4–Cl41 89(1)
C41–Ru4–Cl42 93(1)
C41–Ru4–N41 176(1)
C41–Ru4–N42 93(1)
C42–Ru4–Cl41 94(1)
C42–Ru4–Cl42 87(1)
C42–Ru4–N41 91(1)

C42–Ru4–N42	174(1)
Cl42–Ru4–Cl41	177.6(3)
N41–Ru4–Cl41	87.6(5)
N41–Ru4–Cl42	90.1(5)
N41–Ru4–N42	86.4(6)
N42–Ru4–Cl41	90.6(4)
N42–Ru4–Cl42	88.3(4)

Selected dihedral angles (°)

$[D_3(N21)]$–$[T_4]$	88.6(5)
$[D_3(N31)]$–$[T_4]$	85.2(5)

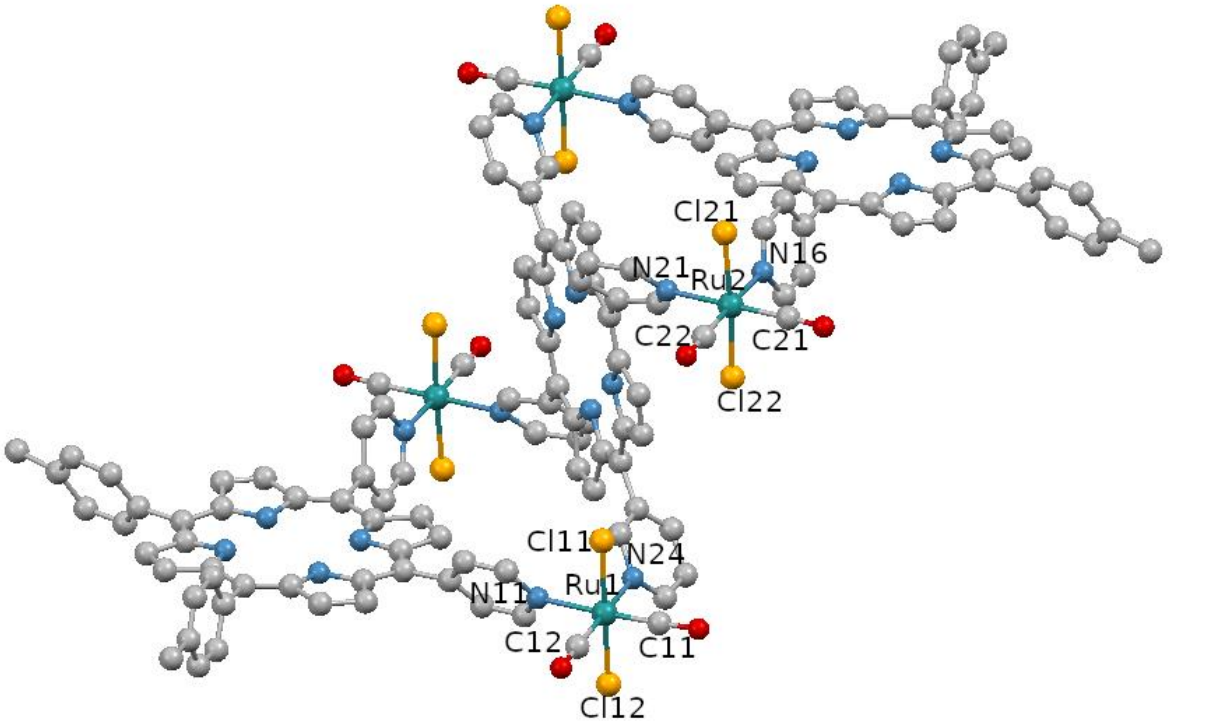

Figure S32. The X-ray molecular structure of stereoisomer $(\mathbf{D_4}\text{-}\mathbf{T_3}\text{-}\mathbf{D_4})_z$ (side view) with numbering scheme. The hydrogen atoms have been omitted for clarity.

Table S3. Selected coordination distances (Å) and angles (°) for $(\mathbf{D_4}\text{-}\mathbf{T_3}\text{-}\mathbf{D_4})_z$ (see Figure S32).

Selected distances (Å)	
Ru1–C11	1.75(2)
Ru1–C12	1.846(17)
Ru1–Cl11	2.395(5)
Ru1–Cl12	2.400(5)
Ru1–N11	2.168(12)
Ru1–N24	2.135(12)
Ru2–C21	1.876(18)
Ru2–C22	1.884(17)
Ru2–Cl21	2.413(5)
Ru2–Cl22	2.387(5)
Ru2–N16	2.163(12)
Ru2–N21	2.142(11)

Selected angles (°)	
C11–Ru1–C12	90.3(6)
C11–Ru1–Cl11	88.9(6)
C11–Ru1–Cl12	90.9(6)
C11–Ru1–N11	178.0(7)
C11–Ru1–N24	92.7(5)
C12–Ru1–Cl11	95.0(6)
C12–Ru1–Cl12	86.8(6)
C12–Ru1–N11	90.7(5)
C12–Ru1–N24	174.8(6)
Cl11–Ru1–Cl12	178.18(12)
N11–Ru1–Cl11	89.3(4)
N11–Ru1–Cl12	90.9(4)
N24 –Ru1–Cl11	89.4(4)
N24–Ru1–Cl12	88.8(4)
N24–Ru1–N11	86.4(4)
C21–Ru2–C22	86.8(6)
C21–Ru2–Cl21	91.4(7)
C21–Ru2–Cl22	91.0(7)
C21–Ru2–N21	177.4(5)
C21–Ru2–N16	92.2(6)
C22–Ru2–Cl21	90.8(6)
C22–Ru2–Cl22	87.4(6)
C22–Ru2–N21	95.5(5)
C22–Ru2–N16	177.3(7)

Cl22–Ru2–Cl21	176.90(13)
N16–Ru2–Cl21	91.8(5)
N16–Ru2–Cl22	90.1(5)
N21–Ru2–Cl21	89.6(4)
N21–Ru2–Cl22	88.1(4)
N21–Ru2–N16	85.4(5)

Selected dihedral angles (°)

$[D_4]$–$[T_3]$	77.6(4)